SACLANTCEN REPORT
serial no.: SR-137

SACLANT UNDERSEA RESEARCH CENTRE

REPORT

The numerical simulation of infrared satellite measurements over the Greenland–Iceland–Norwegian Sea

P.J. Minnett

June 1988

This document is released to a NATO Government at the direction of SACLANT Undersea Research Centre subject to the following conditions:

- The recipient NATO Government agrees to use its best endeavours to ensure that the information herein disclosed, whether or not it bears a security classification, is not dealt with in any manner (a) contrary to the intent of the provisions of the Charter of the Centre, or (b) prejudicial to the rights of the owner thereof to obtain patent, copyright, or other like statutory protection therefor.

- If the technical information was originally released to the Centre by a NATO Government subject to restrictions clearly marked on this document the recipient NATO Government agrees to use its best endeavours to abide by the terms of the restrictions so imposed by the releasing Government.

Page count for SR-137
(excluding covers)

Pages	Total
i-iv	4
1-57	57
	61

SACLANT Undersea Research Centre
Viale San Bartolomeo 400
19026 San Bartolomeo (SP), Italy

tel: 0187 540 111
telex: 271148 SACENT I

NORTH ATLANTIC TREATY ORGANIZATION

SACLANTCEN SR-137

The numerical simulation of infrared satellite measurements over the Greenland–Iceland–Norwegian Sea

P.J. Minnett

The content of this document pertains to work performed under Project 23 of the SACLANTCEN Programme of Work. The document has been approved for release by The Director, SACLANTCEN

Peter C Wille
Director

Acknowledgement: Thanks are due to Mr. A.M. Zavody of the Rutherford Appleton Laboratory (RAL) for advice on the use of his radiative transfer model and for supplying the precomputed spectral parameters, and to Dr. D.T. Llewellyn-Jones, Head of Atmospheric Sciences at RAL, for permission to use the model.

The numerical simulation of infrared satellite measurements over the Greenland–Iceland–Norwegian Sea

P.J. Minnett

Abstract: The accuracy with which self-calibrating satellite infrared radiometers can measure sea-surface temperature is limited by the modification of the electromagnetic radiation before it reaches the radiometer. These physical effects are described for the spectral interval of infrared wavelengths from ~ 10 μm to ~ 14 μm and the 'split-window' expression for sea-surface temperature is derived and discussed. An accurate numerical line-by-line model of the radiative transfer through the atmosphere is presented and is used to simulate measurements of the Advanced Very High Resolution Radiometer (AVHRR/2) on the NOAA series of near-polar orbiting satellites for conditions of the region of the Greenland, Iceland and Norwegian Seas. A set of regionally optimised zenith-angle dependent coefficients for the 'split-window' algorithm is derived and its error characteristics are discussed. While the benefit of using such coefficients is demonstrated, the errors resulting from failing to account properly for seasonal changes in this particular region are shown to be relatively small. The FORTRAN programs used for the AVHRR/2 simulations at SACLANTCEN are described in appendixes to the report.

Keywords: atmospheric variability ○ AVHRR ○ GIN Sea ○ radiative transfer ○ satellite infrared radiometers ○ sea-surface temperature.

Contents

1. Introduction

The Advanced Very High Resolution Radiometers (AVHRR) on the current generation of the US polar-orbiting weather satellites of the TIROS-N series, operated by the National Oceanic and Atmospheric Administration (NOAA), are capable of taking temperature measurements with a random noise level of about 0.1 K. Since the AVHRR has on-board radiometric calibration, the mean error of the temperature measurements should be insignificant and the random error could be reduced to well below the 0.1 K level by averaging over many independent measurements. Thus, in principle, such instruments on satellites could provide ocean scientists and meteorologists with a source of sea-surface temperature (SST) measurements of far superior accuracy and coverage than is possible by any other means. The problem, however, is that in its passage through the intervening atmosphere the radiation leaving the sea-surface is significantly modified in a way that is highly variable in space and time. The accuracy of the SST measurements is therefore limited by the accuracy with which the effect of the atmosphere can be corrected.

In the 'thermal infrared' part of the electromagnetic spectrum, where these measurements are made, the atmospheric effect is wavelength dependent (Fig. 1). Thus simultaneous, co-registered measurements at two or more wavelength intervals (channels) provide a mechanism for the real-time correction of the atmospheric effects. In practice the algorithm takes the form of a simple linear combination of the temperatures measured in the different channels, T_i:

$$T_s = a_0 + \sum_{i=1}^{n} a_i T_i, \tag{1}$$

where T_s is the SST measurement, a_i are dimensionless coefficients, n is the number of channels, and a_0 is a constant temperature. The minimisation of errors in the SST measurement is dependent on the correct choice of the coefficients a_0, a_i.

There are two approaches to determine the coefficients and these can be conveniently referred to as the empirical and the simulation methods. The empirical approach requires the collection of high quality measurements from *in-situ* thermometers, such as on drifting meteorological buoys, that are coincident with satellite measurements. Then a regression analysis of the *in-situ* temperatures and the satellite data produces the coefficients. The alternative approach uses a computer model of atmospheric radiative transfer together with a large set of atmospheric profiles to simulate the satellite measurements in a range of conditions. The simulated measurements are then used with the associated SST values to derive the coefficients, again by regression analysis. In both methods, the regression analysis also provides an estimation of the accuracy with which the SST value can be derived.

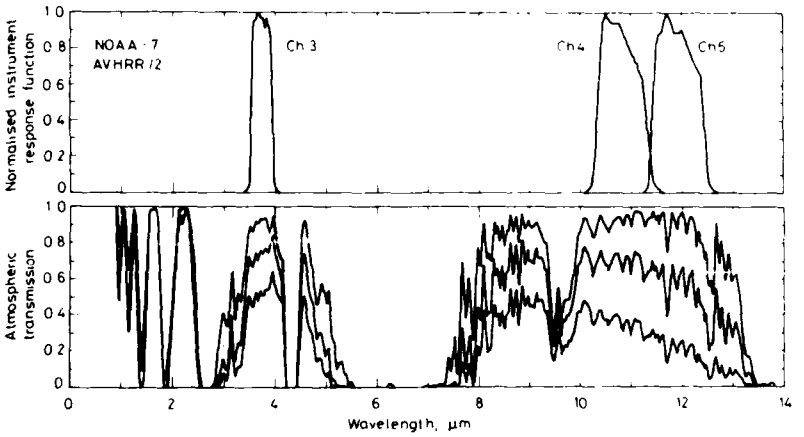

Fig. 1 Theoretical spectra of atmospheric transmission, at nadir, in the infrared wavelength interval of 1 to 14 μm. The three spectra correspond to different amounts of precipitable water (polar: 7 mm; mid-latitude: 29 mm; tropical: 54 mm). Aerosol effects are not included in these spectra. The reponse functions of channel 3 ($\sim$ 3.7 μm), channel 4 ($\sim$ 11 μm) and channel 5 ($\sim$ 12 μm) of the AVHRR/2 on the NOAA-7 satellite are shown, and indicate the 'atmospheric windows' used. The different levels of dependence of atmospheric transmission on the water vapour amount in each 'window' permits an estimate of the atmospheric effect in sea-surface temperature measurement by multichannel methods.

The advantage of the empirical method is that it uses real satellite data and real *in-situ* data in real conditions. It does, however, have some disadvantages:

(a) The satellite measurement is of the radiation temperature, which, after correction for the atmospheric effect, is attributable to the surface 'skin' of the ocean, while the *in-situ* measurement is generally taken at a depth of a few centimetres to a few metres (the so-called 'bulk' temperature). Because of the heat exchange between ocean and atmosphere, the surface skin temperature is generally several tenths of a Kelvin colder than the bulk temperature. This 'skin effect' is highly variable (Robinson, Wells and Charnock, 1984). There are some *in-situ* measurements from research ships taken with radiation thermometers (e.g. Schluessel et al., 1986) but they are quite scarce.

(b) Spatial and temporal variability in the SST field introduces uncertainty into the comparison: the satellite measurement is a near-instantaneous spatial

average whereas the *in-situ* measurement is either a point-sample, a temporal average at a given location, or a temporal and spatial average along a ship's track.

(c) The number of usable coincident sets of measurements is relatively small because many are invalidated by the effects of clouds in the satellite data, and the presence of undetected clouds is a likely source of significant error. Generally, the condition of coincidence must be relaxed to include *in-situ* temperatures taken within several hours of the satellite overpass, thus introducing the possibility of errors caused by temporal or advective temperature changes.

(d) Calibration errors in both the satellite and *in-situ* data are carried over into the SST retrieval expression. This could be considered an advantage if calibration errors in the satellite data are constant, as they would be compensated at each application of the retrieval expression.

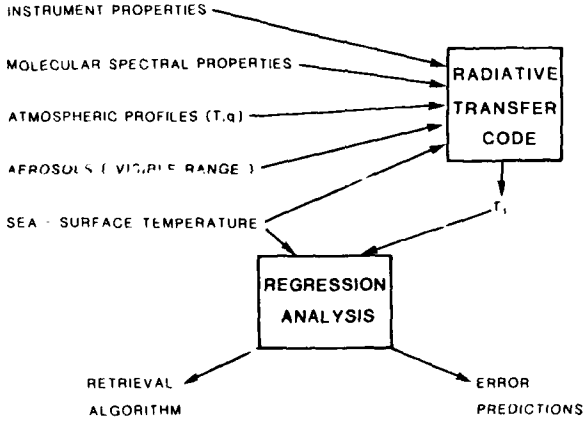

Fig. 2. Block diagram of the procedure for the numerical simulations of satellite radiometric measurements.

The simulation approach is shown schematically in Fig. 2. It avoids all of the problems of the empirical approach, but is prone to disadvantages associated with the model and its input:

(a) Errors can arise through inadequate knowledge of the spectral properties of the atmospheric constituents, and their dependences on temperature and pressure, which is especially relevant to the water vapour 'spectral continuum', and through assumptions necessary in the formulation of the numerical model, such as the effects of aerosols.

(b) Measurement errors in the descriptions of the atmospheric profiles will introduce errors in the simulated satellite data. Random measurement errors in individual profiles are not important, provided the profile remains physical, as the data are used to represent realistic distributions rather than the true state of the atmosphere at the time and location of each profile.

(c) Since the simulations are of skin temperature measurement, the predictions of the modelling, i.e. the coefficients of the retrieval expression and its accuracy, are difficult to verify properly. Discrepancies in predictions and validation data could be caused by several effects which may not be readily identifiable.

The main advantage of the simulation approach is that it permits controlled numerical experiments to investigate the behaviour of the predicted algorithm in response to variations in the input information. In particular, one can study its response to different atmospheric conditions (such as those caused by regional and seasonal variations) or its dependency on particular variables, such as the satellite zenith angle.

The simulation approach is adopted here, largely because of this advantage, but also because it avoids the need for collecting and controlling the quality of large quantities of *in-situ* data. The empirical approach is also rendered unfavourable because the area of interest, the Greenland-Iceland-Norwegian Sea (GIN Sea), is one with a relative paucity of ships and buoys, and this disadvantage is compounded by the relatively high incidence of cloud cover

A line-by-line radiative transfer model with high spectral resolution has recently been implemented at SACLANTCEN to simulate the infrared measurements of AVHRR in the atmospheric 'windows' at about 3 to 4 μm and about 10 to 13 μm in cloud-free conditions. As input the model requires (Fig. 2):

- the spectral properties of the atmospheric constituents which which interact with electromagnetic radiation in these wavelength intervals;
- profiles of atmospheric temperature and humidity characteristic of the conditions of interest;
- the values of the air–sea temperature difference;
- the aerosol concentration in the lower troposphere
- the relevant characteristics of the satellite instruments

The model and its input are described in this report Specific examples of AVHRR

simulations in the GIN Sea are given in the form of an optimised SST retrieval algorithm for use with measurements from the so-called 'split-window' channels at ~ 10 to ~ 13 μm, and a discussion of the algorithm's error characteristics. A more detailed description of the FORTRAN code is given in Appendices A (

2. Radiative transfer in the atmosphere

The energy received by a satellite radiometer directed towards the sea-surface has components originating from the sea, the atmosphere, and the sun (Fig. 3a). In the atmosphere, the processes of absorption, emission and scattering are caused by both molecules and suspended particles, such as dust, water-droplets, ice-crystals and sea-salt crystals. By confining ourselves to a relatively narrow wavelength interval in the infrared part of the electromagnetic spectrum, many of the components illustrated schematically in Fig. 3a can be safely neglected:

(a) the molecular scattering of solar energy into the field of view of a satellite radiometer results in a significant contribution to the signal at visible wavelength, but since the scattering shows approximately a λ^{-4} dependence (Rayleigh Scattering) the effects at the infrared wavelengths of interest (~ 10 to ~ 13 μm) are negligible (see Singh and Warren, 1983).

(b) unlike radiation at visible wavelengths, the infrared radiation leaving the ocean does so from a very thin (< 1 mm) 'skin', so subsurface effects such as scattering by suspended particles can be ignored.

(c) the reflected solar radiation at wavelengths of about 10 μm can be neglected in comparison with the radiation emitted by the sea-surface:

- the solar spectral irradiance is ~ 0.30 W m$^{-2}\mu$m^{-1} at the top of the atmosphere which, assuming a worst-case of 100% atmospheric transmittance, is also the spectral irradiance at the sea-surface;
- the sea-surface spectral emittance at 300 K is ~ 31 W m^{-2} μm^{-1};
- the reflection coefficient at 10 μm is < 0.02 (Friedman, 1969);
- the ratio of reflected solar to surface emitted radiances is therefore $0.30 \times 0.02/31 \simeq 0.0002$;
- at ~ 10 μm the black-body radiance of a source varies as $\sim T^5$.

From these values it can be seen that for a sea-surface temperature of 300 K the apparent increase in temperature due to insolation reflected into the radiometer field-of-view is ~ 0.012 K. This is $\sim 10\%$ of the nominal noise equivalent temperature difference (NEΔT), i.e. the inherent noise level, of the detectors of the AVHRR channels 4 and 5.

(d) even thin clouds in the radiometer field of view prevent the infrared radiation from the sea-surface reaching the height of the spacecraft. Thus, as in the visible wavelength region, the clouds obscure the sea-surface when observed from satellites. Consequently, for the purposes of these simulations it is presumed that effective data analysis techniques exist to identify all pixels in the

infrared image data that contain any cloud; these contaminated pixels must be excluded from the procedure to retrieve sea-surface temperature values.

The remaining components of the radiation received by the satellite radiometer are shown in Fig. 3b and are (a) the radiation emitted at the sea-surface, but modified by its passage through the atmosphere; (b) the radiation emitted by the atmosphere (including aerosols) into the radiometer field of view; and (c) the radiation emitted by the atmosphere (and aerosols) and reflected at the sea-surface into the radiometer field of view.

Throughout the atmosphere, emission and absorption are dependent on the local temperature, on the density of aerosols, on the density of molecular types composing the gaseous atmosphere, and on the spectral properties of those molecules, which in turn are temperature and pressure dependent.

The atmospheric molecules of interest are water vapour (H_2O), carbon dioxide (CO_2), ozone (O_3), nitrous oxide (N_2O) and methane (CH_4).

For the simulations described in this report, the atmospheric temperature and humidity structure is described by sets of radiosonde profiles (Minnett, Eyre and Pescod, 1986 and 1987), but profiles from other sources, such as from satellite-borne atmospheric sounders, or Standard Atmospheres or even synthetic profiles could be used.

The density of aerosols exhibits much spatial and temporal variability and must be well described for the purposes of the simulations. In the cases discussed here only tropospheric aerosols in the lowest 1 km of the atmosphere are considered, and these are parameterised in terms of the sea-level horizontal meteorological range (see Sect. 6). The similarity in size between the wavelength of the infrared radiation and some aerosol particles means that they can be effective scatterers. Assuming the aerosol particles to be spherical, Mie theory can be used to calculate extinction coefficients for a variety of aerosol types and concentrations (Kneizys et al., 1980). In conditions where the density of aerosols is sufficiently high for multiple scattering to be important, it is assumed that the cloud detection algorithms of a sea-surface temperature retrieval procedure would identify such cases as not being 'clear-atmosphere' measurements. Consequently, multiple scattering by aerosols is neglected here.

With the exception of water vapour, the atmospheric gases listed above can be considered 'well-mixed' throughout the atmosphere and not to exhibit significant seasonal or regional changes. Even though there is a well-documented seasonal variation in the concentration of CO_2 (e.g. Hanson et al., 1981) the amplitude of the seasonal cycle is $< 5\%$ of the mean value of 330×10^{-6}, which is the value used here.

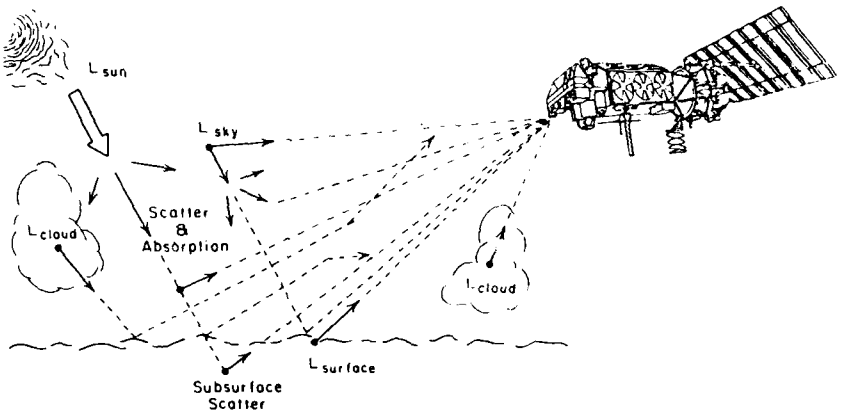

Fig. 3a. Schematic diagram of the physical processes involved in the radiative transfer through the amosphere. In the general case, the satellite radiometer signal has many components from the sun, atmosphere and ocean.

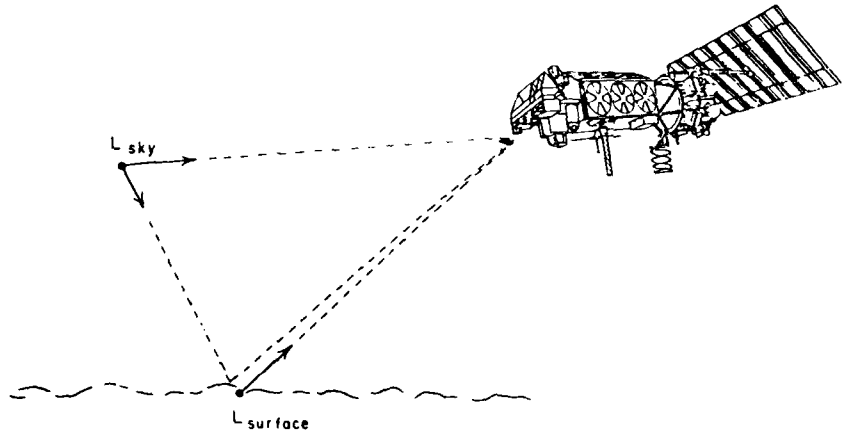

Fig. 3b. Schematic diagram of the physical processes involved in the radiative transfer through the amosphere. In the limited wavelength range of the thermal infrared at $\sim$ 10 to $\sim$ 13 μm, there are only three significant components.

The concentration of atmospheric water-vapour, on the other hand, exhibits extreme variations which must be correctly accounted for in these numerical simulations. As for the temperature profiles, radiosonde ascents are used to provide these data. Water vapour adds a further complication to the simulations, as in addition to the line absorption and emission of infrared radiation by molecular rotation and vibration, it displays quasi-continuous absorption and emission which is dependent on the water-vapour pressure. This has been termed the 'water vapour continuum' and is presumed to be caused by the presence of water vapour dimers, $(H_2O)_2$, and possibly larger water vapour polymers. The continuum effects form an important part of the total atmospheric contribution to the satellite radiometer signal, especially for moist atmospheres—and although there are experimental determinations of the properties of the water vapour continuum, uncertainties in these are likely to contribute a significant component to the inaccuracies in numerical simulations.

2.1. MATHEMATICAL FORMULATION

The change in spectral radiance $L(\nu)$ of a non-divergent, monochromatic beam, at wavenumber ν, when it traverses normally an infinitesimally thin layer of atmosphere, thickness $\mathrm{d}z$ at height z, and within which all properties are uniform and constant, is given by

$$\mathrm{d}L(\nu) = -\kappa(z,\nu)L(\nu)\,\mathrm{d}z \tag{2}$$

where $\kappa(z,\nu)$ is the absorption coefficient of that layer. This is Bouguet's Law.

The atmosphere in the layer $\mathrm{d}z$ is also emitting radiation into the beam, $\mathrm{d}L_e(\nu)$, which, assuming local thermodynamic equilibrium, is equal to the local absorption, by Kirchoff's Law,

$$\mathrm{d}L_e(\nu) = \kappa(z,\nu)L_A(z,\nu,T_A)\,\mathrm{d}z, \tag{3}$$

where $L_A(z,\nu,T_A)$ is the blackbody spectral radiance at the local atmospheric temperature T_A, and L_A is related to temperature T by Planck's Law,

$$L_A(T,\nu)\,\mathrm{d}\nu = B(T,\nu)\,\mathrm{d}\nu = \frac{2h\nu^3\,\mathrm{d}\nu}{c^2(e^{h\nu/kT}-1)}, \tag{4}$$

where h is Planck's constant, k is Boltzmann's constant and c is the speed of light in vacuum.

Thus,

$$\frac{\mathrm{d}L}{\mathrm{d}z} = L_A(z,\nu,T_A)\kappa(z,\nu) - L(z,\nu)\kappa(z,\nu). \tag{5}$$

Solving this linear differential equation using the conditions at the sea-surface, $z = 0$, and the height of the satellite, $z = H$, results in

$$L_H(\nu) = L_0(\nu)\exp\left[-\tau(0,H)\right] + \int_0^H L_A(z,\nu,T_A)\kappa(z,\nu)\exp\left[-\tau(z,H)\right]\mathrm{d}z, \tag{6}$$

where $L_H(\nu)$ is the spectral radiance measured at the satellite, $L_0(\nu)$ is the upwelling spectral radiance at the bottom of the atmosphere and

$$\tau(z_1, z_2) = \int_{z_1}^{z_2} \kappa(z')\,\mathrm{d}z', \tag{7}$$

is the optical thickness of the layer $z_2 - z_1$. When $z_1 = 0$ and $z_2 = H$, τ is the optical depth of the atmosphere.

The term $L_0(\nu)$ is the sum of the radiation emitted by the sea-surface at temperature T_s, i.e. $L_s(T_s, \nu)$, and the reflected downwelling atmospheric radiation, $r(\nu)L\downarrow(\nu)$, where $r(\nu)$ is the spectral reflectance of the sea-surface. Hence

$$L_0(\nu) = L_s(T_s, \nu) + r(\nu)L\downarrow(\nu). \tag{8}$$

But

$$L_s(T_s, \nu) = \epsilon(\nu)B(T_s, \nu), \tag{9}$$

where $\epsilon(\nu)$ is the emissivity of the sea-surface, which is related to the spectral reflectance through Kirchoff's Law,

$$r(\nu) = 1 - \epsilon(\nu). \tag{10}$$

Thus

$$r(\nu)L\downarrow(\nu) = \big(1 - \epsilon(\nu)\big) \int_H^0 L_A(z, \nu, T_A)\kappa(z, \nu) \exp\big[-\tau(z, 0)\big]\,\mathrm{d}z. \tag{11}$$

In reality the channels of a satellite radiometer are not monochromatic, but have a finite width (see Fig. 1). Thus in order to simulate real satellite measurements it is necessary to integrate the spectral radiance at satellite heights, $L_H(\nu)$ in Eq. (6), across the width of the channel, using $\phi_i(\nu)$, the spectral response for channel i, to give the channel radiance L_i,

$$L_i = \int_0^\infty L_H(\nu)\phi_i(\nu)\,\mathrm{d}\nu \Big/ \int_0^\infty \phi_i(\nu)\,\mathrm{d}\nu. \tag{12}$$

In the general case, when the beam does not propagate normally to the atmospheric stratification (which is assumed to be locally horizontal), but at a local zenith angle θ, the thickness of the infinitesimal layer $\mathrm{d}z$ must be replaced by $\sec\theta\,\mathrm{d}z$. This approximation, which neglects the changing refractive index through the atmospheric column, is valid for $\theta < 60°$; for larger zenith angles a more complicated expression should be used (e.g. Kondratyev, 1969).

2.2. MULTICHANNEL ATMOSPHERIC CORRECTIONS

Without detailed knowledge of the condition of the atmosphere, it is not possible to solve the radiative transfer problem (Eqs. (6), (8), (11) and (12)) and thereby derive the sea-surface temperature T_s from a radiance measurement at a single wavenumber interval, or channel, L_i. However, inspection of atmospheric transmission spectra for various atmospheric conditions (Fig. 1) reveals differing dependencies at different parts of the spectra. For example, the change in the atmospheric transmission in going from dry, cold, arctic conditions to warm, moist, tropical ones is more pronounced in the wavelength interval 11.5 to 12.5 μm (i.e. close to AVHRR channel 5) than 10 to 11 μm (i.e. close to AVHRR channel 4). This spectral dependence implies that coincident measurements at different spectral intervals (channels) can be used to correct for the effect of the atmosphere, and hence to measure the sea-surface temperature, without recourse to ancillary measurements of the atmospheric profiles.

In developing the mathematical expression for the correct form of the combination of the multi-channel measurements to derive T_s, it is usual to simplify the problem by first neglecting the contribution of the reflected downwelling atmospheric radiation (Anding and Kauth, 1970; Prabhakara et al., 1974; McMillin, 1975). This leads to a simplified expression:

$$L(\bar{\nu}_i) = B(\bar{\nu}, T_i^s)\tau_0(\bar{\nu}_i) + \overline{B}_A\Big(1 - \tau_0(\bar{\nu}_i)\Big), \tag{13}$$

where $\bar{\nu}_i$ is a mean wavenumber for the spectral interval defined by the normalised channel i response function

$$\bar{\nu}_i = \int_0^\infty \nu\hat{\phi}_i(\nu)\,\mathrm{d}\nu \tag{14}$$

with

$$\int_0^\infty \hat{\phi}(\nu)\,\mathrm{d}\nu = 1. \tag{15}$$

T_i^s is an effective sea-surface radiation temperature, incorporating the effects of the surface emissivity, sometimes called the grey-body temperature, i.e.

$$B(\bar{\nu}_i, T_i^s) = \int_0^\infty \epsilon(\nu)B(\nu, T_s)\hat{\phi}_i(\nu)\,\mathrm{d}\nu. \tag{16}$$

$\tau_0(\nu_i)$ is the atmospheric transmission at channel i, and $\overline{B}_A(\bar{\nu}_i, \overline{T}_{Ai})$ is a weighted mean atmospheric emission at temperature $\overline{T}_{Ai}$,

$$\overline{B}_A(\bar{\nu}_i, \overline{T}_{Ai}) = \frac{\displaystyle\int_{\tau_0(\nu_i)}^1 \int_0^\infty B(\nu, T_A(z))\hat{\phi}_i(\nu)\,\mathrm{d}\nu\,\mathrm{d}\tau}{\displaystyle\int_{\tau_0(\nu_i)}^1 \mathrm{d}\tau}. \tag{17}$$

The neglect of the downwelling atmospheric radiation, $L\downarrow(\nu_i)$ is, in fact, an unnecessary assumption as the form of Eq. (13) can be retained by defining an effective upwelling surface temperature T_i^* such that

$$B(\bar{\nu}_i, T_i^*) = \int_0^\infty \left[\epsilon(\nu)B(\nu, T_s) + r(\nu)L\downarrow(\nu)\right]\dot{\phi}(\nu)d(\nu). \tag{18}$$

Rearranging Eq. (13) gives

$$L(\bar{\nu}_i) = B(\bar{\nu}_i, T_i^*) - \left(B(\bar{\nu}_i, T_i^*) - \bar{B}_A\right)\left(1 - \tau_0(\bar{\nu}_i)\right). \tag{19}$$

Now assuming that T_i^* and $\overline{T}_{Ai}$ are close so that the Planck functions can be related by

$$B(\bar{\nu}_i, \overline{T}_{Ai}) = B(\bar{\nu}_i, T_i^*) + \frac{\partial B}{\partial T}(\overline{T}_{Ai} - T_i^*), \tag{20}$$

then Eq. (18) can be recast in terms of temperature

$$\begin{aligned} T_i &= T_i^* - \left(1 - \tau_0(\bar{\nu}_i)\right)\left(T_i^* - B^{-1}\left[B(\bar{\nu}_i, \overline{T}_{Ai}) + \frac{\partial B}{\partial T}(\overline{T}_{Ai} - T_i^*)\right]\right) \\ &\simeq T_i^* - \left(1 - \tau_0(\bar{\nu}_i)\right)\left(1 + \frac{\partial B}{\partial T}\right)(T_i^* - \overline{T}_{Ai}), \end{aligned} \tag{21}$$

where T_i is the temperature equivalent to the satellite radiance measurement in channel i, sometimes called the brightness temperature

Assuming that the atmospheric transmission can be functionally related to path length (or quantity of absorbing substances, which is mainly water vapour, q) and atmospheric temperature, then

$$(1 - \tau_0(\bar{\nu}_i)) \simeq \kappa_0(\bar{\nu}_i) f_i(q) g_i(T), \tag{22}$$

where $\kappa_0(\bar{\nu}_i)$ is an effective absorption coefficient: f_i and g_i are functions of water vapour density and atmospheric temperature.

Thus,

$$T_i = T_i^* + c_i\kappa_0(\bar{\nu}_i)\left(T_i^* \quad T_A(\bar{\nu}_i)\right), \tag{23}$$

where c_i is a value which is constant for given atmospheric conditions.

Considering now measurements made at two channels ($i = 1, 2$) chosen such that

$$T_A(\bar{\nu}_1) \simeq T_A(\bar{\nu}_2),$$

then

$$\frac{T_1^*(1+\xi_1)-T_1}{\xi_1} \simeq \frac{T_2^*(1+\xi_2)-T_2}{\xi_2}, \tag{24}$$

where $\xi_i = c_i\kappa_0(\bar{\nu}_i)$.

Rearranging terms gives

$$T_1^*(1+\xi_1)\xi_2 - T_2^*(1+\xi_2)\xi_1 = \xi_2 T_1 - \xi_1 T_2.$$

Expressing the surface radiation temperature at the two channels in terms of the surface thermodynamic temperature,

$$T_i^* = \hat{T}_s - \delta_i, \tag{25}$$

where $\hat{T}_s$ is the estimate of sea-surface temperature derived from T_1, T_2, gives

$$\hat{T}_s(\xi_2 - \xi_1) = \delta_1\xi_2(1+\xi_1) - \delta_2\xi_1(1+\xi_2) + \xi_2 T_1 - \xi_1 T_2, \tag{26}$$

i.e.

$$\hat{T}_s = a_0 + a_1 T_1 + a_2 T_2. \tag{27}$$

This is the simple expression for the multichannel measurement of sea-surface temperature $\hat{T}_s$ from two coincident measurements T_1 and T_2 at different wavelength intervals.

Some authors (e.g. McMillin and Crosby, 1984) reduce the retrieval expression to a single coefficient χ to give

$$\hat{T}_s = T_1 + (T_1 - T_2)\chi, \tag{28}$$

where

$$\chi = \frac{\xi_1}{\xi_2 - \xi_1},$$

which is equivalent to imposing

$$\begin{aligned} a_0 &= 0, \\ a_1 + a_2 &= 1 \end{aligned} \tag{29}$$

In reality these conditions do not hold (e.g. Llewellyn-Jones et al., 1984; McMillin and Crosby, 1984, 1985) and the use of expression (28) in preference to (27) will lead to a loss of accuracy in the retrieved value of $\hat{T}_s$.

The multichannel technique can be extended to more channels, in which case Eq. (27) becomes Eq. (1).

In order to accommodate some of the physical effects assumed to be negligible for the derivation of the multichannel expression, Eq. (27) can be considered the first terms of a higher-order series:

$$\hat{T}_s = a_0 + a_1 T_1 + a_2 T_2 + b_1 T_1^2 + b_2 T_2^2 + \cdots . \tag{30}$$

However, in reality it is found that $b_i \simeq 0$, and, since the satellite measurements inevitably contain inherent noise, the inclusion of higher-order terms does not significantly increase the accuracy of the retrieval of $\hat{T}_s$.

2.3. SEA-SURFACE TEMPERATURE RETRIEVAL AS AN INVERSE PROBLEM

The retrieval of sea-surface temperature from multichannel satellite measurements can be considered as a special example of the general inverse problem of retrieving geophysical variables from remotely sensed data. Thus, without detailed consideration of the physics of the radiative transfer, the form of the retrieval expression can be simply derived.

In a recent paper, Eyre (1987) has dealt with the much more complex problem of retrieving atmospheric profiles of temperature and humidity from simultaneous measurements from many (i.e. 18) infrared and microwave channels. What follows below is an application of part of Eyre's general discussion to the specific retrieval of sea-surface temperature.

The linear inversion of satellite radiance measurements can be expressed by

$$\hat{\mathbf{x}} - \mathbf{x}_0 = W(\mathbf{y}_m - \mathbf{y}_0), \tag{31}$$

where $\hat{\mathbf{x}}$ is the retrieved vector; $\mathbf{x}_0$ is the first-guess vector; $\mathbf{y}_m$ is the vector of satellite measurements; $\mathbf{y}_0$ is the measurement vector corresponding to $\mathbf{x}_0$ and W is the inverse matrix.

In the n-channel sea-surface temperature problem, the vector $\hat{\mathbf{x}}$ simply becomes the retrieved variable $\hat{T}_s$ and $\mathbf{y}_m$ is the vector T_i, $i = 1, n$. In a non-iterative approach to solving Eq. (31), the inverse matrix W can be determined by a 'minimum variance' criterion in which the retrieval error for a large number of cases would be minimised. The first-guess vectors $\mathbf{x}_0$ and $\mathbf{y}_0$ in such an instance could be the climatological mean values of surface temperature and corresponding satellite measurements for the atmospheric conditions in which W is valid. In the linearised problem, the measurement vector $\mathbf{y}_m$ is related to the true vector $\mathbf{x}_T$ by

$$\mathbf{y}_m - \mathbf{y}_0 = K(\mathbf{x}_T - \mathbf{x}_0) + \boldsymbol{\varepsilon}, \tag{32}$$

where K is the matrix of partial derivatives of the elements in $\mathbf{y}_m$ with respect to those in $\mathbf{x}_T$, evaluated at $\mathbf{x}_0$, and $\boldsymbol{\varepsilon}$ is the vector of the measurement errors.

Combining Eqs. (31) and (32) gives

$$\hat{\mathbf{x}} - \hat{\mathbf{x}}_0 = R(\mathbf{x}_T - \mathbf{x}_0) + W\boldsymbol{\varepsilon}, \tag{33}$$

where

$$R = WK. \tag{34}$$

Expressing the retrieval in terms of a difference from the true vector $\mathbf{x}_T$,

$$\hat{\mathbf{x}} - \mathbf{x}_T = (\mathbf{1} - R)(\mathbf{x}_0 - \mathbf{x}_T) + W\boldsymbol{\varepsilon}, \tag{35}$$

where $\mathbf{1}$ is the unit matrix, leads to a simple relationship for the mean error characteristics of the retrieved variables

$$\overline{\hat{\mathbf{x}} - \mathbf{x}_T} = (\mathbf{1} - R)\overline{(\mathbf{x}_0 - \mathbf{x}_T)} + \overline{W\boldsymbol{\varepsilon}}. \tag{36}$$

For a well-designed, well-calibrated instrument it is reasonable to assume that the measurement errors $\boldsymbol{\varepsilon}$ are randomly distributed with zero mean—in which case the final term is zero. Thus the mean retrieval errors will be zero if

$$R = \mathbf{1}, \tag{37}$$

and/or

$$\overline{\mathbf{x}_0 - \mathbf{x}_T} = 0. \tag{38}$$

In the general case, argues Eyre, condition (37) will not hold, and minimization of mean errors requires close correspondence between the first-guess vectors used in the retrieval and the true vectors. This is an important, if intuitive, result but does not tell us anything about the form of the retrieval expression. If, for the specific case of interest here we assume (37) to hold, and remembering the definition of R (Eq. (34)), then the elements of R are given by

$$r_{ik} = \sum_{j=1}^{n} w_{ij}\kappa_{jk} = \begin{cases} 1 & \text{for } i = k \\ 0 & \text{for } i \neq k. \end{cases} \tag{39}$$

For the multichannel SST retrieval problem, the matrices collapse to vectors ($i = k = 1$), thus

$$\sum_{j=1}^{n} w_j k_j = 1, \tag{40}$$

where w_j are the coefficients of the retrieval and $k_j = \mathrm{d}T_j/\,\mathrm{d}T_s$, i.e.

$$\sum_{j=1}^{n} w_j\,\mathrm{d}T_j/\,\mathrm{d}T_s = 1, \tag{41}$$

which gives, on integration,

$$T_s = w_0 + \sum_{j=1}^{n} w_j T_j, \tag{42}$$

where w_0 is the constant of integration. This is the simple multichannel retrieval expression (Eq. (1)) and, for $n = 2$, Eq. (27).

2.4. THE 'SPLIT-WINDOW' RETRIEVAL

The transfer functions for the infrared channels of the NOAA-7 satellite AVHRR/2 are shown in Fig. 1 above atmospheric transmission spectra for three atmospheric profiles representative of different regions. There are slight differences between the channel transfer functions from satellite to satellite. The channels are positioned in 'atmospheric windows', i.e. where the atmosphere is relatively transparent, so that at least some of the energy received at the satellite comes from the sea-surface. For the simulations considered here the two channels of interest are 4 and 5, which share the atmospheric 'window' at 10 to 13 μm. Thus they are sometimes called the 'split-window' channels. Their proximity supports the assumptions needed to linearise the radiative transfer problem and derive the multi-channel retrieval expression, which can be written

$$T_s = a_0(\theta) + a_4(\theta)T_4(\theta) + a_5(\theta)T_5(\theta), \tag{43}$$

where the numerical subscripts 4 and 5 are the channel numbers, and θ is the local zenith angle to the satellite sensor measured at the sea-surface. The zenith angle dependence is required not only because of the changes in atmospheric path length across the instrument swath, but also because of the dependence of the sea-surface emissivity ϵ on emission angle. The surface emissivity, weighted by the normalised channel transfer functions, is smaller for channel 5 than for channel 4 at all emission angles.

The atmosphere is generally cooler than the ocean surface below and as a result the brightness temperatures measured in space are usually lower than the sea-surface temperature. Further, since the atmosphere is less transparent for channel 5 than for channel 4, the atmospheric contribution to the channel 5 signal is greater and thus T_5 is cooler than T_4. Meteorological situations do arise where the reverse is true, and these are caused by warm, moist layers in the atmosphere being advected over a cooler ocean surface. However, cases with $T_5 > T_4$ are quite rare as the atmospheric temperature inversion has also to overcome the effect of the lower surface emissivity at channel 5, as well as the effects of the inevitably colder atmosphere above.

3. The radiative transfer model

The computer model used here is derived from a general radiative transfer code developed at the Rutherford Appleton Laboratory of the UK Science and Engineering Research Council, and made specific for the spectral intervals of the 'atmospheric windows' at about wavelengths 3.5 to 4.0 μm and 10 to 13 μm, which are used by AVHRR/2 (see Fig. 1).

The model simulates the atmospheric radiative transfer as described by Eqs. (6), (8), (11) and (12), but with the integrals replaced by summations over discrete intervals. The wavenumber increment is 0.04 cm^{-1} and the height integrals are recast in terms of pressure increments.

The atmosphere is considered to consist of 128 plane-parallel layers of uniform pressure intervals of about 8 mbar. The precise pressure resolution is dependent on the value of the surface pressure. For the simulation of measurements through atmospheric paths at zenith angle θ, the thickness of each layer is multiplied by $\sec\theta$.

Atmospheric profiles are required by the model in the form of a two-dimensional array containing values of height (km), pressure (mbar = hPa), air temperature (K), moist air density ($\mathrm{g\,m}^{-3}$) and water vapour density ($\mathrm{g\,m}^{-3}$). These can be readily calculated from, for example, the measurements of radiosonde ascents. It is important that the profiles used in the simulations extend to great height, as they are extrapolated to the satellite altitude (i.e. zero pressure). While this is reasonable for profiles that reach, say 50 mbar or less (i.e. heights > 20 km) those profiles that are truncated at lower levels can give erroneous or unphysical extrapolated values. This risk is particularly great for profiles truncated at levels where there are still variations in the water vapour density.

Measurements of atmospheric temperature and humidity profiles are much more numerous than those of aerosol properties. Consequently it is necessary to adopt a model of the aerosol distribution and properties. For the simulations discussed here it is assumed that the aerosols are confined to the lowest kilometre of the atmosphere (which is similar to some assumptions used elsewhere, e.g. Kneizys et al., 1980), and that the aerosol extinction (i.e. scattering plus absorption) coefficient β is scaled by the sea-level horizontal meteorological range V as given by the Koschmieder formula

$$V = \frac{1}{\beta}\ln\eta^{-1} = 3.912/\beta, \tag{44}$$

where the coefficient β is for a reference wavelength of 0.55 μm and has units km^{-1}, and η is a constant, set to 0.02. Alternatively, if β is expressed in $\mathrm{dB\,km}^{-1}$,

$$V = 16.99/\beta. \tag{45}$$

Throughout the lower kilometre the extinction coefficient is itself scaled by the measured profile of relative humidity u according to the results of Hänel (1976),

$$\beta \propto \left(\frac{1 - u}{1 - u_0} \right)^m , \tag{46}$$

where u_0 is the relative humidity at sea-level, and m is a constant, set to 0.4. To extend these expressions to the wavelength intervals of interest here (3.5 to 4.0 μm, and 10 to 13 μm) the normalised extinction coefficient $\dot{\beta}_\lambda$ at 3.7 and 11 μm for the marine aerosol type of the LOWTRAN5 code were used (Kneizys et al, 1980: Appendix A, pp. 180–183) to give

$$\dot{\beta}_\lambda = \frac{16.99}{V} \left(\frac{1 - u}{1 - u_0} \right)^{0.4} \dot{\beta}_\lambda . \tag{47}$$

A similar expression is used to obtain the aerosol emission coefficients.

At the 10 to 13 μm wavelength interval, aerosol effects are much less important than at shorter wavelengths, so the simulations are relatively insensitive to inadequacies in the aerosols model. It has been shown elsewhere (Minnett, 1986) that for the atmospheric conditions typical of the mid-latitude summer, changing the meteorological range from 100 km to 23 km changes the predicted brightness temperatures, T_4 and T_5, by less than about 0.4 K. This is to be compared with mean temperature deficits (for 100 km range) of 1.8 K (for $T_s - T_4$) and 2.7 K (for $T_s - T_5$).

The model treats each spectral line in the atmospheric 'window' individually, i.e. it is a line-by-line model, as opposed to band models in which only the mean properties of all the spectral lines of a larger wavenumber interval (say 20 or 40 cm^{-1}) are considered. The band models obviously require less computing time, but are inevitably less accurate.

The spectral data describing the radiative attenuation of the atmospheric gases have been precalculated at each wavenumber increment at five standard levels in the atmosphere. These are at pressures of 1000, 800, 600, 400, 200 mbar, with corresponding temperatures of 290, 280, 270, 250 and 220 K. The properties of each spectral line have been taken from the US Air Force Geophysics Laboratory compilation (Rothman, 1987), using the Gross (1955) line shape for collision broadening. All spectral lines within 20 cm^{-1} wavenumbers of each wavenumber increment are considered. A total of 908 lines are used for the wavenumber interval for AVHRR/2 channel 4 and 925 for channel 5. The channel 4 interval begins at 853.76 cm^{-1}, and has 3656 increments, and channel 5 at 800.00 cm^{-1} with 2222 increments. At each wavenumber increment and at each of the five standard levels, the attenuation coefficient and its temperature dependence (parameterised in terms of a quadratic function of temperature difference) have been calculated and stored as two sets of values, one for water vapour and the other for the well-mixed gases. The quadratic

parameterizations are used to calculate the attenuations at the measured temperature, but at the nearest two of the standard pressures. Then linear interpolation, or extrapolation, in pressure provides the required attenuation at the measured temperature and pressure.

The water vapour dimer attenuation, the so-called continuum or anomalous attenuation, is derived from a parameterization of the form:

$$\tau_2 = \alpha \rho_w^2 \exp\left[\gamma/(T - T_0)\right], \tag{48}$$

where α is an empirically determined quadratic function of wavenumber (Bohlander, 1979), ρ_w is the water vapour density, γ is a constant, T is the measured temperature and T_0 is a reference temperature (296 K).

The atmospheric attenuation at each wavenumber and pressure increment is then calculated as the sum of those from the water vapour monomer, the water vapour dimer, mixed gases and aerosols.

By summing the effects at each pressure increment the model can now produce three spectra for each atmospheric profile: the atmospheric attenuation, the upwelling atmospheric radiance at the satellite height and the downwelling atmospheric radiance at the bottom of the atmosphere. These are independent of the sea-surface temperature itself, and of the properties of the particular satellite radiometer.

The next step in the simulation is to calculate the emission from the sea-surface in the required wavenumber interval at a given sea-surface temperature (Eq. (9)), and combine this with the model outputs to give the upwelling radiance spectrum at the satellite height (Eq. (6)). Since the air-sea temperature difference is a variable quantity, it is legitimate to use a set of SST values with each atmospheric profile. The choice of SST values should, of course, be guided by geophysical constraints (see Sect. 5).

Finally, the simulated satellite radiance measurement is derived by summing the product of the calculated upwelling radiance at each wavenumber increment and the corresponding element of the normalised channel response function. The result can be expressed as the channel brightness temperature (T_4 or T_5) by inverting the Planck function, taking into account the channel response function, which can best be achieved using a pre-calculated 'look-up table'.

For the purposes of retrieval algorithm development, the simulations of the satellite measurements are done for a large set of atmospheric profiles, each with a range of air-sea temperature differences, to provide a representative set of T_4, T_5 and T_s. It has been shown that to adequately describe the range of atmospheric and oceanic conditions in a regional and seasonal study about 500 sets of simulated measurements are required (Minnett, 1986). This requires at least 100 independent profiles

to correctly sample the atmospheric variability, each with five different air-sea temperature differences.

The coefficients for the split window retrieval expression (Eq. (43)) can then be determined by simple linear regression analysis, which also provides a prediction of the *standard error* of the retrieved sea-surface temperature. The regression procedure, however, must take into account the possibility of inherent noise in the radiometer channels (which can be assumed to have a gaussian distribution about zero mean). The derived retrieval coefficients a_i are thus dependent on the radiometer noise levels and will be smaller for particularly noisy channels.

4. Atmospheric profiles

The profiles of atmospheric temperature and moisture used here have been measured by radiosonde ascents, and are a subset of North Atlantic area profiles selected from the extensive archive at the UK Meteorological Office (Minnett, Eyre and Pescod, 1986 and 1987). The profiles were selected from the seven year period of December 1975 to November 1982 and collected into monthly sets for marine and continental conditions (24 sets). In this study, only the marine data sets have been used, consisting of quality-controlled profiles for each month of the year, originating from Ocean Weather Stations (OWS), islands and coastal weather stations.

The initial selection was restricted to profiles which extended to pressure levels of 15 mbar or less and included moisture information (dew point temperature) to 600 mbar or less. The profiles were required to be physically reasonable and then subjected to a statistical filter (3σ rejection) at 40 pressure levels. A radiation transfer model was then used to generate synthetic radiances at satellite altitudes, which were also required to be physically reasonable. Further details of the selection and quality control procedures are given by Pescod and Eyre (1983). The main source of error was found to be mistakes in the coding of the raw radiosonde data.

The data for each profile consist of pressure, temperature and dew point temperature at both the standard reporting levels and special levels. The special levels, sometimes called significant points, are those at which gradients change, so by joining the special level data with straight lines (on a tephigram), the measured profile can be correctly described. Profiles reconstructed using both the special level and standard level data have been used here.

One of the initial selection criteria was that the lowest-level pressure measurement (P_0) be $\geq$ 1000 mbar. This was to ensure that the interpretation of computed correlations throughout the atmospheric column should not be confused by changes resulting from a reduced number of samples at P_0 = 1000 mbar. For the North Atlantic area as a whole this restriction does not introduce a significant sampling bias (see, for example, the charts of Isemer and Hasse, 1985), but, however, this may not be the case in the GIN Sea area—particularly during winter. For example, at OWS 'M' (66°N, 2°E) there is about an 8% probability of $P_0 < 1000$ mbar during May, but in December the probability has increased to about 48% (US Naval Weather Service Command, 1974a). For some applications this bias could be disturbing, while for others the bias towards anticyclonic conditions with an increased likelihood of reduced cloud cover may reflect more appropriate sampling for infrared remote sensing. The consequence of this sampling bias on the AVHRR simulations will be investigated when more radiosonde profiles taken in cyclonic conditions are available.

The original monthly sets of marine atmospheric profiles consist of 400 ascents covering the area from about 30°N to 80°N, within a range of about 3000 km of the UK. For the purpose of simulating AVHRR/2 measurements in the GIN Sea area, radiosondes from stations north of 58°N and between 40°W and 20°E were selected. The number of radiosondes in each of the resulting monthly sets is given in Table 1, together with the mean values and standard deviations of some of the relevant atmospheric parameters, which are also shown graphically in Fig. 4. It can be seen that February is the month with the driest atmosphere and coldest mean surface air temperature, with July being the moistest and warmest. Profiles from these two months were selected to investigate the benefits of seasonal SST retrieval algorithms for AVHRR measurements (see Subsect. 8.2).

Table 1
Monthly characteristics of the GIN Sea marine atmosphere

Month	Number of profiles	Precipitable water ($kg\ m^{-2}$)	Surface specific humidity ($g\ kg^{-1}$)	Surface air temperature (°C)
Jan	146	7.13 ± 3.82	3.16 ± 1.24	-0.02 ± 4.59
Feb	183	6.26 ± 3.08	2.84 ± 1.10	-0.72 ± 4.75
Mar	148	6.46 ± 3.36	3.02 ± 1.23	-0.15 ± 6.52
Apr	175	7.31 ± 3.50	3.41 ± 1.40	1.22 ± 6.13
May	186	10.54 ± 5.13	4.42 ± 1.61	4.74 ± 5.78
Jun	148	15.31 ± 6.19	5.96 ± 1.86	8.74 ± 5.11
Jul	183	17.06 ± 5.14	6.57 ± 1.60	9.88 ± 4.26
Aug	190	16.44 ± 5.75	6.43 ± 1.78	9.42 ± 4.48
Sep	167	13.69 ± 6.12	5.41 ± 1.92	7.12 ± 4.87
Oct	191	9.90 ± 4.88	4.24 ± 1.61	4.52 ± 4.88
Nov	127	7.84 ± 4.15	3.48 ± 1.53	1.60 ± 5.17
Dec	136	7.00 ± 3.55	3.18 ± 1.42	0.32 ± 4.74

Figure 5 shows the mean temperature and humidity profiles, with the envelope of ± 1 standard deviation, for these months. These have been calculated after interpolating each measured profile to uniform pressure levels at 15 mbar resolution. The distributions of some surface variables are shown for these months as histograms in Fig. 6.

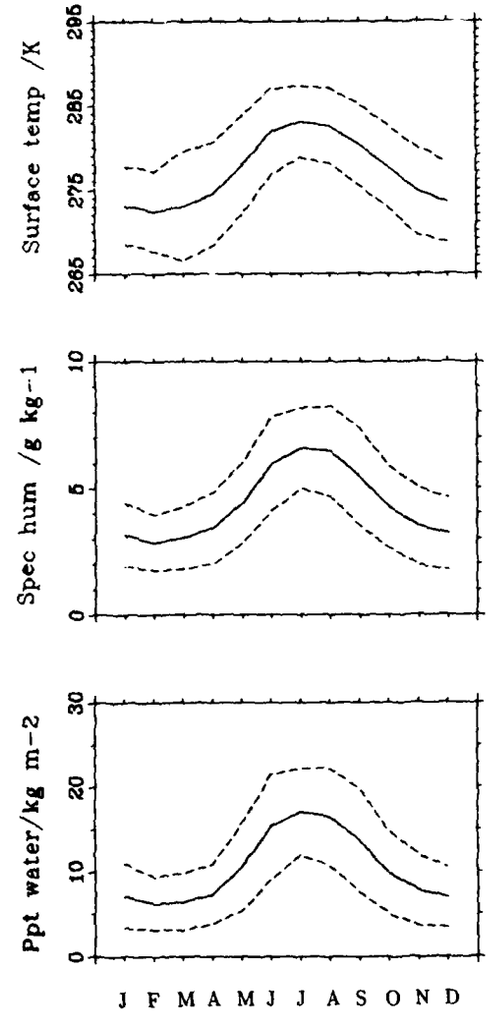

Fig. 4. Annual cycles of some of the atmospheric properties in the GIN Sea area. These are shown as monthly means ±1 standard deviation derived from radiosonde measurements. The variables are surface air temperature, surface specific humidity, and atmospheric water vapour column content (precipitable water). The numerical values are given in Table 1.

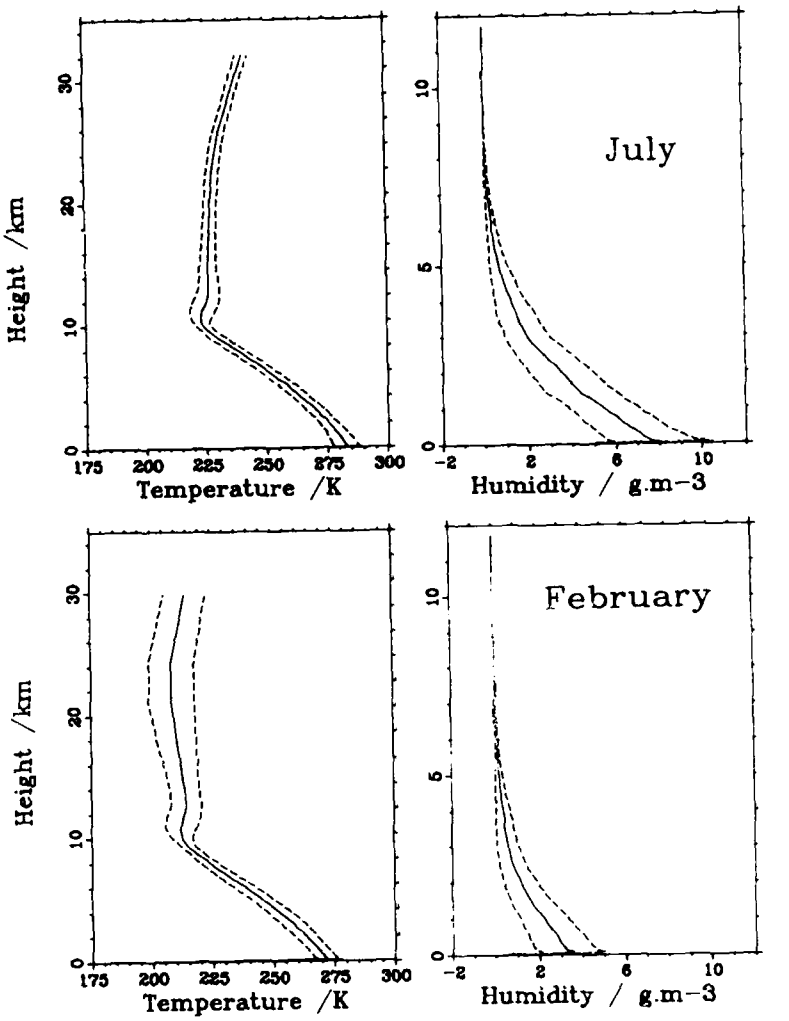

Fig. 5. Atmospheric profiles of temperature and absolute humidity for the summer (July) and winter (February) conditions in the GIN Sea area. The profiles are shown as mean values ±1 standard deviation for 15 mbar pressure increments of radiosonde profiles. The envelopes of ±1 standard deviation are exclusive for the two months.

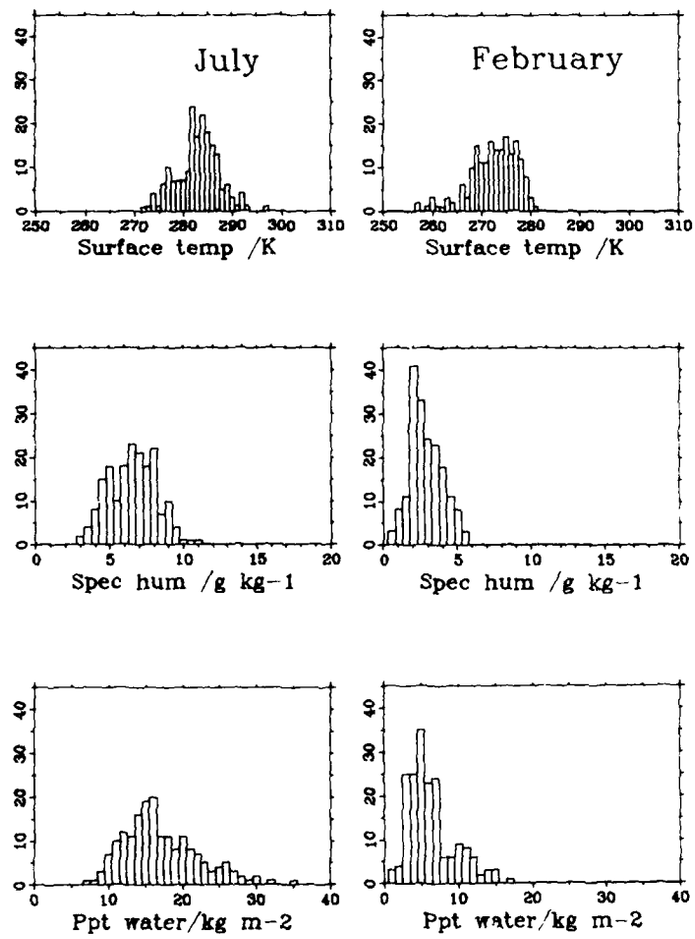

Fig. 6. Histograms of some of the atmospheric properties in the GIN Sea area for summer (July) and winter (February). The variables are surface air temperature, surface specific humidity and water vapour column content (precipitable water). The data are derived from radiosonde measurements.

5. Air–sea temperature differences

Since the atmosphere is generally colder than the ocean surface beneath, the brightness temperatures measured in space are generally colder than the temperature of the sea-surface. The size of this temperature deficit is strongly dependent on the difference between the surface air temperature and the SST. Furthermore, the retrieval coefficients optimised to give zero mean error when applied to measurements taken in a specific range of atmospheric conditions are themselves dependent on the air–sea temperature differences encountered in those conditions. Thus, for the simulations to be accurate, realistic air–sea temperature differences must be used. (Unfortunately the radiosonde profiles used here do not include the associated SST measurement).

The air–sea temperature difference field in most of the GIN Sea area is poorly sampled, especially in the winter months. An exception to this is the OWS 'M' at 66°N, 2°E, and monthly statistics of surface meteorological variables are presented in graphic and tabular form by the US Naval Weather Service Command (1974a,b). Inspection of the tables for air-sea temperature differences for February and July (ibid., 1974b) reveals that there are two distinct regimes in winter and summer. In February the SST is largely independent of surface air temperature, with low air temperatures being accompanied by large air–sea temperature differences: when the air temperature decreases, in the mean by 6.66 K, the SST is reduced by only 0.74 K. In July, however, a decrease in air temperature of 4.44 K is accompanied by an SST drop, in the mean, of 2.30 K. Such behaviour is to be expected given the larger thermal inertia of the deeper surface mixed layer in winter.

For the AVHRR simulations, it is appropriate therefore, to associate each atmospheric profile with a set of SST values independent of the air temperature for February, but to have sets of air–sea temperature differences which are dependent on the air temperature for July.

While it is reasonable to expect the distinct winter and summer regimes identified in the OWS 'M' data to hold for the GIN Sea area as a whole, the SST values themselves at OWS 'M' during February are patently inappropriate for other parts of the area: the mean SST being 6.5°C, with a standard deviation of only 0.7 K. This means, assuming a gaussian distribution, that less than 1% of observations would be colder than 4.4°C, which is obviously not applicable in the northwest of the area towards the ice-edge. Consequently, in what follows, SST values of −1.0°C, 1.0°C, 3.0°C, 5.0°C and 7.0°C are used with each atmospheric profile of the Fel ruary simulations.

For the July simulations the air–sea temperature differences shown in Table 2 are used with each atmospheric profile. The values are derived from the OWS 'M' data

(ibid., 1974b), and since they are related to the surface air temperature of each profile, are assumed applicable to the GIN Sea area as a whole.

Table 2
Air-sea temperature differences used in the July simulations

Surface air temperature (°C)	Air-sea temperature differences (K)				
≤ 9.0	−3.0	−2.5	−2.0	−1.5	−1.0
> 9.0 ≤ 11.5	−1.5	−1.0	−0.5	0.0	0.5
> 11.5	−1.0	−0.5	0.0	0.5	1.0

6. Tropospheric aerosols

Since the radiosonde profiles contain no information about the aerosol distribution in the atmosphere, a parameterisation of aerosol effects in terms of the meteorological range is used (Eq. (47)). Estimates of visibility form part of the routine synoptic meteorological observations and their statistics have been compiled (UK Meteorological Office, 1964; US Naval Weather Service Command, 1974a,b). For the GIN Sea area, the available statistics are dominated by the observations from OWS 'M' (66°N, 2°E), which show that when there is no precipitation (a necessary condition for infrared remote sensing) nearly half ($\sim$ 44%) of the observations have visible range $>$ 30 n.mi, i.e. $>$ 55 km (UK Meteorological Office, 1964). This is also the case for the smaller number of reports from Jan Mayen Island (ibid.). The monthly mean visibilities at OWS 'M' show some seasonal dependence with values of 10–12 n.mi (18–22 km) in winter compared to 20 n.mi (37 km) in early summer. These mean values are for all observations, however, and probably merely reflect the winter increase in the frequency of precipitation (Gathman, 1985) when infrared remote sensing is impossible.

However, the 'visibility', which is subjectively determined, is not the same as the quantitative 'meteorological range' required for the Koschmieder formula (Eq. 44), the relationship between the two being

$$V = (1.3 \pm 0.3) V_{\mathrm{obs}}, \tag{49}$$

where V_{obs} is the observed visibility (Kneizys et al., 1980).

For the simulations reported here, a meteorological range of 50 km has been used, which corresponds to an observed visibility of 30–50 km (17–26 n.mi). In this respect the simulations will be of less favourable conditions than the mean, and the predicted residual errors may be even somewhat pessimistic.

7. The Advanced Very High Resolution Radiometer

The Advanced Very High Resolution Radiometer (AVHRR) is a five-channel imaging device which forms part of the payload of the TIROS-N series of polar-orbiting weather satellites. There are two such satellites in operation at any time (currently NOAA-9 and NOAA-10) in sun-synchronous orbits; one overhead at about 0230 UTC and 1430 UTC, and the other at about 0730 UTC and 1930 UTC. The satellites are about 840 km above the sea-surface and have orbital periods of ~ 100 minutes. The channel characteristics are given in Table 3. However, it should be noted that the instruments on TIROS-N, NOAA-6, NOAA-8 and NOAA-10 are without channel 5.

Table 3
Channels of the Advanced Very High Resolution Radiometer, AVHRR

Channel	Wavelength (μm)	Signal
1	~ 0.6 to ~ 0.7	reflected solar energy – clouds, coastlines, vegetation
2	~ 0.7 to ~ 1.1	reflected solar energy – clouds, coastlines, vegetation
3	~ 3.5 to ~ 4.0	reflected solar and thermal emission – clouds, SST
4	~ 10.3 to ~ 11.3	thermal emission – SST, clouds
5	~ 11.5 to ~ 12.5	thermal emission – SST, clouds

The infrared channels are in the so-called 'atmospheric windows' where the atmosphere is relatively transparent (Fig. 1), so that most of the signal originates from the surface. The two longwave channels are at wavelengths close to the peak of the Planck function for emitted energy at terrestrial temperatures, and are used primarily for sea-surface temperature determination. Unlike these, the 3.7 μm channel is susceptible to contamination by reflected solar radiation during the day, and so it is used for sea-surface temperature measurements only when the viewing geometry is such that the solar contamination is impossible, or at least unlikely, or during the night. Data from this channel are useful in detecting and classifying clouds both during night and day. The two shortwave channels are also used for cloud-detection

and for delineating coastlines. They are also used to determine the 'vegetation index' over land.

The AVHRR data stream includes measurements in the infrared channels of an on-board black-body calibration target and of space (zero radiance measurement). The temperature of the black-body, which is close to terrestrial temperatures, is monitored by four platinum resistance thermometers. The noise levels in the two longwave channels is low, being given as 0.12 K for a 300 K target, but in reality they appear to be much lower. The 3.7 μm channels, however, have had much higher noise levels, often worsening with the age of the instrument. The data from each channel are digitised for 10-bit resolution (0–1023). The spatial resolution at nadir is 1.1 km and the swath width is about 3150 km.

Information about the instrumental properties is published by NOAA as each new satellite becomes operational. The spectral response functions of the channels vary from instrument to instrument, which has a consequence on the SST retrieval expressions (see Subsect. 8.4).

Detailed descriptions of the AVHRR instrument and data stream are given by Schwalb (1978) and Lauritson et al. (1979).

8. Results of GIN Sea simulations

The results of the simulations of the AVHRR 'split-window' measurements for conditions over the Greenland–Iceland–Norwegian Seas are presented in this section. Sea-surface temperature retrieval coefficients are derived and their error characteristics are discussed. While the numerical values presented are particular to the GIN Sea conditions, the qualitative conclusions will be applicable to regional studies in general.

The values of the simulated brightness temperatures for February (winter conditions) and July (summer conditions) are given in Table 4 as mean values and standard deviations for four different zenith angles (measured at the sea-surface).

Table 4
Simulated NOAA-9 AVHRR measurements[a] over GIN Sea

Zenith angle ($\theta°$)	$\sec\theta$	T_s (°C)	T_4 (°C)	T_5 (°C)	$T_4 - T_s$ (K)	$T_5 - T_s$ (K)
February						
0.0	1.00	3.000 ± 2.831	1.915 ± 2.693	1.550 ± 2.635	-1.085 ± 0.195	-1.450 ± 0.290
41.4	1.33	3.000 ± 2.831	1.554 ± 2.653	1.079 ± 2.581	-1.446 ± 0.253	-1.921 ± 0.368
53.1	1.67	3.000 ± 2.831	0.855 ± 2.604	0.209 ± 2.520	-2.145 ± 0.318	-2.791 ± 0.454
60.0	2.00	3.000 ± 2.831	-0.027 ± 2.554	-0.933 ± 2.460	-3.027 ± 0.393	-3.933 ± 0.563
July						
0.0	1.00	10.516 ± 3.627	8.941 ± 3.445	8.333 ± 3.382	-1.575 ± 0.435	-2.183 ± 0.631
41.4	1.33	10.516 ± 3.627	8.489 ± 3.415	7.772 ± 3.359	-2.027 ± 0.548	-2.744 ± 0.773
53.1	1.67	10.516 ± 3.627	7.799 ± 3.418	6.985 ± 3.388	-2.717 ± 0.647	-3.531 ± 0.890
60.0	2.00	10.516 ± 3.627	7.033 ± 3.454	6.117 ± 3.468	-3.483 ± 0.734	-4.399 ± 0.991

[a] The temperatures and temperature differences are given as mean ± standard deviation of 500 values, derived from simulations using 100 atmospheric profiles, each with 5 air–sea temperature differences.

The temperature deficits are also given in Table 4. The simulated values agree with physical expectations, in that

(a) $T_5 < T_4$,

(b) the temperature deficits become more negative with increasing zenith angles,

(c) temperature deficits are more negative for summer conditions, when the atmospheric water vapour burden is greater, and

(d) the variability of the temperature deficits is greater for channel 5 than for channel 4, reflecting the increased contribution of the atmosphere to the channel 5 signal. For both channels the variability of the brightness temperatures is much greater than of the temperature deficits, indicating that most of the signal does, as expected, come from the sea. That the variances of the brightness temperatures are smaller than for the sea-surface temperature confirms that the presence of the atmosphere attenuates the appearance of surface temperature gradients.

8.1. REGIONALLY OPTIMISED SEA-SURFACE TEMPERATURE RETRIEVALS

The simulated channel brightness temperatures for the winter and summer conditions were regressed against the corresponding sea-surface temperatures to derive the retrieval coefficients optimised for the GIN Sea area. These are given in Table 5. The channel transfer functions of the NOAA-9 AVHRR were used. A noise equivalent temperature difference (NEΔT) of 0.02 K was assumed for both channels in all cases, which is smaller than the single pixel value of 0.12 K (see Sect. 7). The coefficients are optimised for the conditions used in the simulations in that they produce a zero mean SST retrieval error and minimised standard error. Provided that the conditions of the simulations accurately reflect the environmental conditions of the GIN Sea, they are optimised for use in that area. Also given in Table 5 is the estimate of the standard error of the retrievals, which is smallest for measurements at nadir ($\theta = 0°$). Because of the low value for the NEΔT used in the deviation, it would be necessary to average the derived SST values over several pixels (> 36) to achieve these error values in practice.

In order to determine whether the effort of deriving regional coefficients is worthwhile, a globally applicable set of retrieval coefficients was applied to the GIN Sea simulations. The global coefficients are those used by NOAA for the operational generation of SST maps, known as the MCSST (multi-channel sea-surface temperature) maps, and are derived by regressing real satellite data with *in-situ* measurements from drifting buoys (see Strong and McClain, 1984; McClain et al., 1985). Two different sets of MCSST coefficients are necessary for use with day-time and night-time data. This reflects different satellite data processing schemes (i.e. in the identification of cloud contaminated pixels) for the two types of data, and possibly also the increased net heat loss from the ocean during the night, which follows from the use of a bulk sea temperature in the coefficient derivation. The MCSST coefficients are given in Table 6 together with the mean errors when they are applied to the GIN Sea simulations. For winter conditions near-zero mean error is found for large zenith angles, where the long atmospheric path length and lower surface emissivity combine to produce conditions closer to those for which the MCSST coefficients

Table 5

GIN Sea area sea-surface temperature[a] retrieval coefficients (channels 4 and 5 of NOAA-9 AVHRR/2)

$\sec\theta$	a_0	a_4	a_5	σ (K)
February conditions				
1.00	0.567	2.334	−1.314	0.09
1.33	0.689	2.539	−1.516	0.11
1.67	1.028	2.721	−1.694	0.12
2.00	1.502	2.723	−1.686	0.15
July conditions				
1.00	0.279	3.059	−2.054	0.12
1.33	0.336	3.248	−2.239	0.15
1.67	0.621	3.420	−2.402	0.17
2.00	0.951	3.553	−2.522	0.25

[a] The coefficients are for temperatures expressed as °C.

are applicable. For the warmer, moister summer atmosphere, these conditions are reached at smaller zenith angles. The main result, however, is that the use of global retrieval coefficients can result in mean errors of up to 0.5 K or more.

8.2. SEASONAL DEPENDENCE

The seasonal variations in the atmospheric temperature and humidity profiles are sufficiently great for the envelopes of ± one standard deviation about the mean profile to be exclusive (Fig. 5). This is true also of the marine atmosphere over the N.E. Atlantic as a whole (Minnett, Eyre and Pescod, 1987). This seasonal variation suggests that there may be an advantage in having seasonally optimised coefficients. However, although such seasonal coefficients are significantly different from each other, the seasonal atmospheric variability is not sufficiently great for the improvement in accuracy to really justify their use. This can be illustrated by applying the February coefficients to the July simulations and vice-versa, the results of this test being shown in Table 7. The mean errors that result are small, indicating that regionally optimised coefficients are robust over the range of atmospheric conditions experienced in the course of the seasonal cycle.

Table 6

Regional and zenith angle dependences: mean temperature[a] errors from applying global (MCSST) coefficients to GIN Sea simulations (NOAA-9)

	$\sec\theta$	ΔT	
		(day)	(night)
February	1.00	0.40	0.24
	1.33	0.34	0.21
	1.67	0.11	−0.03
	2.00	−0.07	−0.21
July	1.00	0.44	0.43
	1.33	0.28	0.27
	1.67	−0.14	−0.15
	2.00	−0.15	−0.64
	MCSST coefficients		
	a_0	a_4	a_5
day	5.19	3.6446	−2.6616
night	0.70	3.7028	−2.7040

[a] All temperature errors are in K. The coefficients are for temperatures expressed in °C.

Table 7

Seasonal dependence: temperature[a] errors caused by applying February coefficients to July simulations (NOAA-9)

$\sec\theta$	Mean	σ
1.00	−0.02	0.18
1.33	−0.05	0.22
1.67	−0.10	0.24
2.00	−0.17	0.33

[a] All temperature errors are in K.

8.3. ZENITH ANGLE DEPENDENCE

The need to account for the zenith-angle dependence of the retrieval coefficients in accurate SST measurement has been stressed by a number of authors, particularly Llewellyn-Jones et al. (1984). Indeed, Saunders (1967) found that, for airborne measurements, increasing the zenith angle from 0° to 60° practically doubled the temperature deficit and thereby provided a mechanism for correcting for the atmospheric effect.

The consequence of failing to account for the changing zenith angles across the swath is already apparent in the discussion of the global algorithm (Table 6), but in order to investigate the magnitude of the effect in the case of optimised coefficients, each set of coefficients for the four zenith angles used in the simulations were applied to every set of simulated brightness temperatures. The resulting errors are shown in Table 8, which illustrates that failure to account properly for the zenith angle dependence can lead to unacceptable errors.

Table 8

Zenith angle effects: mean sea-surface temperature[a] errors from failure to account for zenith angle dependency (channels 4 and 5 of NOAA-9, July conditions)

Simulations ($\sec\theta$)	Coefficients ($\sec\theta$)			
	1.00	1.33	1.67	2.00
1.00	0.00	0.21	1.67	1.19
1.33	−0.27	0.00	0.17	1.00
1.67	−0.76	−0.48	0.00	0.53
2.00	−1.32	−1.03	−0.54	0.00

[a] All temperatures are in K.

In reality the effects of zenith angle change smoothly across the swath, which suggests that a functional dependence on zenith angle of the retrieval might be expected. However there are two factors involved: the increasing atmospheric path length with increasing zenith angle, and the decrease in surface emissivity with increasing emission (or zenith) angle, which in turn changes the effective air–sea temperature difference. Thus for the general case where the atmosphere is cooler than the sea-surface, the effective air–sea temperature difference becomes less negative away from the centre of the swath. The relative contributions of the emissivity and atmosphere to the mean temperature deficit are shown for the February simulations in Table 9, from which it can be seen that, in this case, the emissivity effects are dominant.

Table 9
Zenith angle effects: surface emissivity and atmosphere for February conditions

$\sec\theta$	$T_s - T_4$ (K)	ϵ	δT_ϵ (K)[a]	δT_a (K)[b]
Channel 4				
1.0	1.085	0.990	0.57	0.52
2.0	3.027	0.960	2.29	0.74
Channel 5				
1.0	1.450	0.986	0.86	0.59
2.0	3.933	0.947	3.32	0.61

[a] δT_ϵ = temperature drop due to deviation from unity of surface emissivity, ϵ.
[b] δT_a = temperature drop due to atmospheric effects.

In order to demonstrate that for the GIN Sea area at least, the zenith angle dependence of the optimised retrieval coefficients is adequately described by a choice of four zenith angles, a set of simulations for $\sec\theta=1.50$ were made. The errors resulting from applying coefficients for this zenith angle derived by linear interpolation between $\sec\theta=1.33$ and $\sec\theta=1.67$ were calculated and are shown in Table 10. These errors are small enough to be neglected, and if a higher order expression is used for the interpolation then the interpolation errors will be yet smaller.

Table 10
Zenith angle effects: errors from interpolating coefficients at $\sec\theta = 1.50$

	a_0	a_4	a_5	ϵ (K)[a]	σ (K)
February					
Simulated	0.796	2.637	−1.612	-	0.114
Interpolated	0.859	2.630	−1.605	0.059	-
July					
Simulated	0.411	3.338	−2.324	-	0.171
Interpolated	0.479	3.335	−2.321	0.065	-

[a] Mean error in applying interpolated coefficients to simulated brightness temperatures.

Provided the retrieval algorithm is free of non-linear terms, it does not matter whether the coefficients are interpolated before the SST is calculated, or SSTs are calculated at standard zenith angles and then interpolated to that of the measurement. For some computers, especially those with vector arithmetic, it is more efficient to interpolate a set of coefficients for the zenith angle of each pixel across the swath, and apply these to the data scan-line by scan-line. This must of course be done before the image is remapped to any other coordinate system.

8.4. INSTRUMENTAL DEPENDENCE

The channel response functions vary from instrument to instrument: sometimes by design to improve the performance of the AVHRR, and at others unintentionally through slight variations in the properties of filters and detectors. For example, the NOAA-9 AVHRR channel transfer functions are shifted slightly to higher wavenumbers compared with those of NOAA-7: by ~ 5 cm^{-1} for channel 5 and ~ 2 cm^{-1} for channel 4. The widths of the corresponding channels are similar for each instrument, but the positions of local maxima (i.e. peak transmissions) have changed for channel 5. The net effect is that the same radiance measured by the two instruments corresponds to different temperatures. The NOAA-9 channel 4 is about 0.2 K colder than NOAA-7, and this difference is practically independent of temperature, while channel 5 is about 0.2 K warmer for a measurement at 310 K, but the difference decreases to zero at about 270 K.

It is generally accepted that different retrieval coefficients are required for each instrument and hence, for example, new sets of MCSST coefficients are issued for each satellite. The loss of accuracy resulting from failing to account for the different satellite characteristics can be quantified by applying coefficients derived using the NOAA-7 transfer functions to the NOAA-9 simulations. The errors for the July simulations at $\sec\theta$=1.33 are shown in Table 11, and are comparable to those resulting from failure to account for the seasonal dependence at the same zenith angle (Table 7).

Table 11

Spacecraft dependence: temperature[a] errors from applying NOAA-7 coefficients to NOAA-9 simulations (July)

$\sec\theta$	Mean	Range
1.33	0.22	-0.16 to 0.72

[a] All temperatures are in K.

9. Summary and conclusions

The measurements of the AVHRR thermal infrared channels (4 and 5 at $\sim$ 10 to $\sim$ 13 μm wavelength) have been simulated by a line-by-line radiative transfer model using realistic atmospheric and oceanic parameters characteristic of the GIN Sea region. The computer model itself has been previously validated (Llewellyn-Jones et al., 1984) in that sea-surface temperature retrieval coefficients for North Atlantic conditions, derived entirely from the model simulations, produced SST values with realistic error characteristics (i.e. mean error $\sim$ 0.1 K, rms $\sim$ 0.6 K) when compared with *in-situ* data from research ships. These errors are comparable, if not better, than those of other sets of retrieval coefficients found in the literature. Furthermore, the zenith angle dependence of the coefficients from the model agree with physical expectations (McMillin and Crosby, 1985).

The simulations have been used to derive sea-surface temperature retrieval coefficients that are optimised for the winter (February) and summer (July) conditions of the GIN Sea area. The retrieval coefficients have an explicit zenith angle dependence to account for the changing surface emissivity and atmospheric path length across the swath.

A number of approaches for improving the error characteristics of satellite-derived SSTs in a regional study have been explored, and the benefits of each have been quantitatively assessed to determine their relative merits. These approaches are, in the order in which they improve the error characteristics:

(1) Zenith angle dependence. Failure to account for the dependence of the retrieval coefficients can lead to mean errors in excess of 1 K if, for example, coefficients derived for near-nadir measurements are applied to measurements towards the edge of the swath. The zenith angle effects, in the cases studied here, are dominated by those of the changing surface emissivity, with the effects caused by increased atmospheric path length being much less important. It is sufficient to derive the retrieval coefficients at only four distinct zenith angles (e.g. $\sec^{-1}$ 1.00, 1.33, 1.67 and 2.00 have been used here) and interpolate to all other zenith angles. Linear interpolation appears to be adequate. Admittedly some sets of coefficients (such as those of the MCSST) are intended for application to data in a reduced range of zenith angles, close to nadir, but in geographical areas where cloud cover can severely restrict the number of occasions when the sea-surface can be sampled (such as the GIN Sea area) the luxury of discarding cloud-free parts of the image because they lie towards the edges of the swath can be ill-afforded.

(2) Regional dependence. The application of coefficients intended for global use in a regional study, such as of the GIN Sea area, can result in mean errors in

excess of 0.5 K. The errors show a distinct zenith angle dependence.

(3) Seasonal dependence. The failure to account for the seasonal changes in the atmospheric conditions results in quite small mean errors. For example, applying coefficients derived from simulated measurements through the cold, dry atmospheres of February to the simulated data from the (relatively) warm, moist atmospheres of July results in mean errors of only a few tenths of a degree.

(4) Spacecraft dependence. It is generally acknowledged that individual sets of coefficients are required for each instrument, but for the GIN Sea conditions at least, the mean errors that arise when NOAA-7 coefficients are applied to NOAA-9 data are small—being comparable to those caused by the neglect of the seasonal effects.

While much effort has been invested in ensuring that the model and input data provide a realistic representation of the physical world, there is always the risk that some factor is missing or inadequately treated, especially when there are insufficient independent data (such as *in-situ* measurements) with which to conduct a definitive test. Such is the case here. However, the findings discussed above are derived from a coherent set of model simulations which should mean the results are internally consistent. The radiosondes used in the study have been subjected to careful quality control and are used only to describe the atmosphere in a statistical sense, and not to describe the state of the atmosphere at the time and place of measurement of each profile. Thus individual random measurement errors do not invalidate the results. The surface pressure bias in the radiosondes of the winter months (see Sect. 4) is also unlikely to have unduly influenced the results, the only consequence is to have diminished the effects of seasonal changes—but even then, by a factor of probably less than two.

The accuracy required of satellite measurements of sea-surface temperature depends, of course, on the intended applications. For some purposes it may be acceptable to neglect some of the dependences discussed above. But in any event, the merit of using regionally optimised, zenith-angle dependent, split-window coefficients has been clearly demonstrated.

References

ANDING, D. and KAUTH, R. Estimation of sea-surface temperature from space. *Remote Sensing of Environment*, **1**, 1970: 217–220.

BOHLANDER, R.A. Spectroscopy of water vapour. PhD Thesis, University of London, 1979.

EYRE, J.R. On systematic errors in satellite sounding products and their climatological mean values. *Quarterly Journal of the Royal Meteorological Society*, **113**, 1987: 279–292.

FRIEDMAN, D. Infrared characteristics of ocean water (1.5–15μ). *Applied Optics*, **8**, 1969: 2073–2078.

GATHMAN, S.G. Climatology. *In*: HURDLE, B.G. *ed.* The Nordic Seas. New York, NY, Springer, 1985: pp. 1–18.

GRASSL, H. and KOEPKE, P. Corrections for atmospheric attenuation and surface reflectivity in satellite-borne SST measurements. *In*: GOWER, J.F.R. *ed.* Oceanography from Space, New York, NY, Plenum Press, 1981: pp. 97–107.

GROSS, E.P. Shape of collision-broadened spectral lines. *Physical Review*, **97**, 1955: 395–403.

HÄNEL, G. The properties of atmospheric aerosol particles as functions of the relative humidity at thermodynamic equilibrium with the surrounding moist air. *Advances in Geophysics*, **19**, 1976: 73–188.

HANSON, K.J., PETERSON, J.T., NAMIAS, J., BORN, R. and WONG, C.S. On the influence of Pacific Ocean temperatures on atmospheric carbon dioxide concentration at Ocean Weather Station 'P'. *Journal of Physical Oceanography*, **11**, 1981: 905–912.

ISEMER, H.J. and HASSE, L. The Bunker Climate Atlas of the North Atlantic Ocean, Volume 1: Observations. Berlin, Springer, 1985.

KNEIZYS, F.X., SHETTLE, E.P., GALLERY, W.O., CHETWYND, J.H., ABREU, L.W., SELBY, J.E.A., FENN, R.W. and Mc CLATCHEY, R.A. Atmospheric transmittance/radiance: computer code LOWTRAN 5. Report AFGL-TR-80-0067. Hanscom AFB, MA, Air Force Geophysics Laboratory, 1980.

KONDRATYEV, K. Ya. Radiation in the Atmosphere. New York, NY, Academic Press, 1969: pp. 161–171.

LAURITSON, L., NELSON, G.J. and PORTO, F.W. Data extraction and calibration of TIROS-N/NOAA radiometers, NOAA T.M. NESS 107. Washington, D.C., National Oceanic and Atmospheric Administration, 1979.

LLEWELLYN-JONES, D.T., MINNETT, P.J., SAUNDERS, R.W. and ZAVODY, A.M. Satellite multichannel infrared measurements of sea-surface temperature of the N.E. Atlantic Ocean using AVHRR/2. *Quarterly Journal of the Royal Meteorological Society*, **110**,1984: 613–631.

McCLAIN, E.P., PICHEL, W.G. and WALTON, C.C. Comparative performance of AVHRR-based multichannel sea-surface temperatures. *Journal of Geophysical Research*, **90**, 1985: 11587–11601.

McMILLIN, L. Estimation of sea-surface temperatures from two infrared window measurements with different absorption. *Journal of Geophysical Research*, **80**, 1975: 5113–5117.

McMILLIN, L. and CROSBY, D.S. Theory and validation of the multiple window sea surface temperature technique. *Journal of Geophysical Research* **89**, 1984: 3655–3661.

McMILLIN, L. and CROSBY, D.S. Some physical interpretations of statistically derived coefficients for split-window corrections to satellite derived sea surface temperatures. *Quarterly Journal of the Royal Meteorological Society*, **111**, 1985: 867–871.

MINNETT, P.J. A numerical study of the effects of anomalous North Atlantic atmospheric conditions on the infrared measurement of sea-surface temperature from space. *Journal of Geophysical Research*, **91**, 1986: 8509–8521.

MINNETT, P.J., EYRE, J.R. and PESCOD, R.W. The marine atmosphere over the north-eastern Atlantic Ocean: a monthly description of some variables relevant to satellite remote sensing of the ocean and atmosphere. Report RAL-86-044. Chilton, Oxfordshire, UK, Rutherford Appleton Laboratory, 1986.

MINNETT, P.J., EYRE J.R. and PESCOD, R.W. The variability of the North Atlantic marine atmosphere and its relevance to remote sensing. *International Journal of Remote Sensing*, **8**, 1987: 871–880.

PESCOD, R.W. and EYRE, J.R. Accumulation of a set of radiosonde profiles for use with satellite sounding data from the European and North Atlantic areas. Internal report, Met 019 Branch Memo 71. Bracknell, UK, Meteorological Office, 1983.

PRABHAKARA, C., DALU, G. and KUNDE, V.G. Estimation of sea-surface temperature from remote sensing in 11 to 13μm window region. *Journal of Geophysical Research*, **80**, 1974: 5039–5044.

ROBINSON, I.S., WELLS, N.C. and CHARNOCK, H. The sea surface thermal boundary layers and its relevance to the measurement of sea surface temperature by airborne and spaceborne radiometers. *International Journal of Remote Sensing*, **5**, 1984: 19–46.

ROTHMAN, L.S. AFGL atmospheric absorption line parameters compilation: 1980 version. *Applied Optics*, **20**, 1981: 791–795.

SAUNDERS, P.M. Aerial measurements of sea-surface temperatures in the infrared. *Journal of Geophysical Research*, **72**, 1967: 4109–4117.

SCHLUESSEL, P., SHIN, H-Y, EMERY, W.J. and GRASSL, H Comparison of satellite-derived sea-surface temperature with *in-situ* skin measurements. *Journal of Geophysical Research*, **92**, 1987: 2859–2874.

SCHWALB, A. The TIROS-N/NOAA A-G satellite series. NOAA Memo NESS 95. Washington, D.C., National Oceanic and Atmospheric Administration. 1978.

SINGH, S.M. and WARREN, D.E. Sea-surface temperatures from infrared measurements. *In*: CRACKNELL, A.P. *ed.* Remote Sensing Applications in Marine Science and Technology. Dordrecht, the Netherlands, Reidel, 1983: pp. 231–262

STRONG, A.E. and McCLAIN, E.P. Improved ocean surface temperatures from space—comparisons with drifting buoys. *Bulletin of the American Meteorological Society*, **65**, 1984: 138–142.

UNITED KINGDOM. METEOROLOGICAL OFFICE. Weather in Home Fleet Waters, Volume 1 – the Northern Seas, Part 1, M O 732(a). London, HMSO, 1964.

UNITED STATES. NAVAL WEATHER SERVICE COMMAND. Marine Climatic Atlas of the World, Volume 1: North Atlantic Ocean, (NAVAIR 50-1C-528). Washington D.C., US Government Printing Office, 1974a.

UNITED STATES. NAVAL WEATHER SERVICE COMMAND. Summary of synoptic meteorological observations, western European coastal marine areas. Volume 7. Asheville, N.C., National Climatic Center. 1974b.

Appendix A

The radiative transfer code / Program descriptions

The set of computer programs that constitute the model to simulate the satellite measurements are all written in FORTRAN 77. Apart from calls to the subroutines DATE and TIME, to record the start time of execution, there are no VAX-specific statements. Depending on their size, some of the data files are binary and others ASCII; some ASCII files are accessed simply by a READ or WRITE to a logical unit, which needs to be assigned to a file before the programs are run.

A.1. PROGRAM ATRAN

Purpose To calculate the spectrum of atmospheric transmittance given a spectrum of atmospheric attenuation. Also calculates mean atmospheric transmittance.

Input file

name = xxxxxx.ATT
type = binary
access = direct
record length = 1024 real words (4096 bytes)
contents = spectrum of atmospheric attenuation

Output file

name = xxxxxx.TRN
type = binary
access = direct
record length = 1024 real words (4096 bytes)
contents = spectrum of atmospheric transmission

Subroutines DATE, TIME

User dialogue

Prompt – 'Give input file code [6 chars]'
Response – Supply xxxxxx for file names

A.2. PROGRAM BRIEX

Purpose To extract vectors (columns) of variables from two dimensional array of data output by program BRIPM. Output vectors are written to ASCII files in F10.3 format, with one value per record.

Input file

name = FORnnn.DAT; generated by program BRIPM
type = ASCII
contents = 17 columns of data

Output files

name = FORmmm.DAT
type = ASCII
contents = 1 column of data

name = FORyyy.DAT
type = ASCII
contents = log of execution

Subroutines DATE, TIME

User dialogue

Prompt – 'Give input Lu, log Lu'
Response – give logical unit to which input file has been assigned, i.e. *nnn* of FORnnn.DAT; and for an ASCII file which will contain a log of the execution of the program.

Prompt – 'Edit to remove frozen SST? [Y or N]'
Response – Give Y if data cycle (i.e. simulated satellite measurement and associated atmospheric variables) are not to appear in output files when sea-surface temperature is $< -1.9°C$; i.e. the sea-surface is covered by ice.

Prompt – 'Give *number of variables, variable numbers and output lus*'
Response – Input number of variables to be extracted, n, followed by <CR> then n times variable code number (from table in prompt), logical unit for output file.
Note: The variable codes are the following: 1 – month, 2 – profile number, 3 – sea-surface temperature (SST), 4 – brightness T, 5 – temperature deficit, 6 – air temperature, 7 – air temperature – SST, 8 – airmass, 9 – latitude, 10 – longitude, 11 – precipitable water, 12 – surface specific humidity, 13 –

cloud cover, 14 – cloud height, 15 – low cloud type, 16 – medium level cloud type, 17 – high cloud type

A.3. PROGRAM BRIPM

Purpose From output of radiative transfer code (program RADPM) and other information, generates spectra of radiance at the satellite, and of the satellite measurement (i.e. taking into account the channel response function). Also generates a two dimensional array of data of simulated satellite measurements and associated atmospheric parameters.

Input files

name = xxxRS.BIN
type = binary
access = direct
record length = 384 real words (1536 bytes)
contents = atmospheric profiles

name = yyyyyy.UPR
type = binary
access = direct
record length = 1024 real words (4096 bytes)
contents = spectrum of upwelling atmospheric radiance (generated by RADPM)

name = yyyyyy.DNR
type = binary
access = direct
record length = 1024 real words (4096 bytes)
contents = spectrum of downwelling atmospheric radiance (generated by RADPM)

name = yyyyyy.ATT
type = binary
access = direct
record length = 1024 real words (4096 bytes)
contents = spectrum of atmospheric attenuation (generated by RADPM)

name = NaaCHb.TRF
type = binary
access = direct
record length = 1024 real words (4096 bytes)
contents = channel spectral response function for channel 'b' of AVHRR on satellite NOAA-'aa'

name = NaaCHb.RAD
type = binary
access = direct
record length = 1024 real words (4096 bytes)
contents = look-up table to convert radiances measured in channel 'b' of AVHRR on satellite NOAA-'aa' to temperatures (generated by TTORAD)

Output files

name = yyyyyy.RAD
type = binary
access = direct
record length = 1024 real words (4096 bytes)
contents = spectrum of total upwelling radiance at the satellite

name = yyyyyy.CHR
type = binary
access = direct
record length = 1024 real words (4096 bytes)
contents = spectrum of AVHRR channel radiance measurement

name = FORppp.DAT
type = ASCII
contents = two-dimensional array of data (with 17 columns, each with header label)

name = FORqqq.DAT
type = ASCII
contents = log of execution

Subroutines DATE, TIME, INPROF

User dialogue

Prompt – 'Give satellite number, AVHRR channel number, airmass and log LU'
Response – Input one or two digit code ('aa') of NOAA-'aa' satellite name, AVHRR channel number (3, 4 or 5), airmass (i.e. $\sec^{-1}$(zenith angle)), and logical unit to contain log of execution (i.e. qqq of FORqqq.DAT). *Note:* The first three numbers must correspond to those of associated RADPM run.

Prompt – 'Give month of radiosonde data [3 chars]'
Response – Input three-character code, xxx, of name xxxRS.BIN of file containing atmospheric profiles. Must correspond to that used with associated RADPM run.

Prompt – 'Give input file code [6 chars]'
Response – Input yyyyyy of input/output file names. Must correspond to that used with associated RADPM run.

Prompt – 'Give and last radiosondes [as in RADPM run]'
Response – Input number in xxxRS.BIN file of first and last atmospheric profiles used in associated RADPM run.

Prompt – 'Give number of first profile in RADPM output'
Response – Input number of profile in associated RADPM output files (i.e. relative to first profile given in last response) at which processing in this run of BRIPM is to begin. All subsequent profiles to end of data in input files will be processed.

Prompt – 'Number of air temp classes, and number of DTs'
Response – Input the number of classes, divided by air-temperature values (maximum 5) for which air-sea temperature differences will be a constant set, and the number of air-sea temperature differences in each set (maximum 5).

Prompt – 'Give air temp class upper limit, and air-sea DTs'
Response – For each class give upper class limit air temperature and air-sea temperatures for that class. Each class entry is terminated by < CR >, and prompt re-appears.

Comments

(a) Before program is applied for the first time simulations for a new satellite, the CHARACTER*2 array SATNO must be increased in length by one element, and the new satellite identified (i.e. 'aa' of NOAA-'aa') must be entered into SATNO DATA statement.

(b) The sequence of variables in ASCII files is same as listed for program BRIEX.

A.4. PROGRAM RADPM

Purpose Radiative code to calculate spectra of atmospheric radiance, with upwelling at top of atmosphere and downwelling at base of atmosphere, and atmospheric attenuation for simulating measurements of the infrared channels of AVHRR. Aerosols are confined to the lowest kilometre of the atmosphere. The atmospheric profiles are required in the form: H (km), P (mbar), T (K), air density ($g\,m^{-3}$), H_2O density ($g\,m^{-3}$).

Input files

name = xxxRS.BIN
type = binary
access = direct
record length = 384 real words (1536 bytes)
contents = atmospheric profiles

name = ATTCHb.BIN
type = binary
access = direct
record length = 1024 real words (4096 bytes)
contents = Precomputed atmospheric attenuation data in wavenumber interval of AVHRR channel 'b' (=3,4,5).

Output files

name = yyyyyy.UPR
type = binary
access = direct
record length = 1024 real words (4096 bytes)
contents = spectrum of upwelling atmospheric radiance

name = yyyyyy.DNR
type = binary
access = direct
record length = 1024 real words (4096 bytes)
contents = spectrum of downwelling atmospheric radiance

name = yyyyyy.ATT
type = binary
access = direct
record length = 1024 real words (4096 bytes)
contents = spectrum of atmospheric attenuation

Subroutines DATE, TIME, INPROF, FATN, FRHU, FINTP

User dialogue

Prompt – 'Give AVHRR channel number, airmass, visible range/km and log LU'
Response – Input AVHRR channel number (3, 4 or 5), airmass (i.e. $\sec^{-1}$ (zenith angle)), visible range and logical unit to contain log of execution (i.e. qqq of FORqqq.DAT).

Prompt – 'Give month of input data [3 chars]'
Response – Input three-character code, xxx, of name xxxRS.BIN of file containing atmospheric profiles.

Prompt – 'Give output file code [6 chars]'
Response – Input yyyyyy of output file names.

Prompt – 'Give first and last radiosondes'
Response – Input number in xxxRS.BIN file of first and last atmospheric profiles to be used.

Comments The program is structured as a nest of loops. The outermost loop increments for each atmospheric profile, and begins by reading a profile from disk. The next loop increments through wavenumber space across the width of the channel interval. The innermost loop increments up through the height of the atmosphere.

■ *A.4.1. Function* FATN

Purpose Calculates attenuation as H_2O dimer + H_2O monomer + CO_2 absorptions.

Arguments

PR, DT, DD, OH, OC

where

PR = air pressure in mbar
DT = air temperature in K
DD = water vapour density in $g\,m^{-3}$
OH, OC contain values of WATR, CO2A from previous wavenumber calculation, which are used to replace current values if these are negative due to (very rare) breakdown of quadratic approximation of temperature dependence

Common areas

COMMON AA, BE, P(5), T(5), WA(5), CO(5), A(5), B(5), C(5), D(5)

where

AA = anomalous absorption for 1 $g\,m^{-3}$ at reference temperature (scaled)
BE = binding energy, read in eV
TDIF = difference in temperature of layer from temperature used in the absorption calculations
WA(I) = water vapour absorption at temperature T(I) and pressure P(I) [dB km^{-1}]·[$g\,m^{-3}$]$^{-1}$
CO(I) = CO_2 absorption for 1×10^{21} molecules cm^{-2}
A(I), B(I) = linear and 2nd-degree term for H_2O vapour attenuation temperature dependence
C(I), D(I) = linear and 2nd-degree term for CO_2 attenuation temperature dependence

■ *A.4.2. Function* FRHU

Purpose Calculates relative humidity.

Arguments

TE, WD

where

TE = temperature
WD = water vapour density

Common areas None.

■ *A.4.3. Function* FINTP

Purpose Calculates aerosol scaling factors for a given relative humidity, as in LOWTRAN5 (see reference to Kneizys et al., 1980, in main report).

Arguments

RHU, AR(4)

where

RHU = relative humidity
AR contain LOWTRAN5 scaled aerosol cross-sections at 0.55 μm.

Common areas None.

A.5. PROGRAM TTORAD

Purpose Calculates look-up table relating radiance to temperatures in the range 210.0 K to 312.3 K, in increments of 0.1 K, weighted through AVHRR channel response functions. Note that for use with RADPM/BRIPM it is not necessary to renormalise channel response functions. This means that the calculated radiances are not in physical units. In order to generate a table for general use, it is necessary to renormalise the channel response functions.

Input file

name = NaaCHb.TRF
type = binary
access = direct
record length = 1024 real words (4096 bytes)
contents = channel spectral response function for channel 'b' of AVHRR on satellite NOAA-'aa'

Output file

name = NaaCHb.RAD
type = binary
access = direct
record length = 1024 real words (4096 bytes)
contents = look-up table to convert radiances measured in channel 'b' of AVHRR on satellite NOAA-'aa' to temperatures

Subroutines DATE, TIME

User dialogue

Prompt – 'Give satellite number, AVHRR channel number and log LU'
Response – Input one or two digit code ('aa') of NOAA-'aa' satellite name, AVHRR channel number (3, 4 or 5), and logical unit to contain log of execution (i.e. qqq of FORqqq.DAT).

A.6. SUBROUTINE INPROF

Purpose To read radiosonde profile in record IPROF in an open binary data file on logical unit LU. Returns 'radiosonde header' values in array HDR, and atmospheric profiles in arrays H, P, T, RV and RM, which contain 75 elements describing the profile as height (km), pressure (mbar), temperature (K), air density ($g\,m^{-3}$) and water vapour density ($g\,m^{-3}$). Missing data are given value -99.

Arguments

LU, IPROF, IERFL

where

LU = logical unit from which to read profile (file must be opened before INPROF call)
IPROF = number of record containing profile to be read
IERFL = 0 on return if read was successful, else 1.

Common areas

(a) COMMON/PROFIL/H(75), P(75), T(75), RV(75), RM(75) which contain atmospheric profiles (see above)

(b) COMMON/HDPROF/IWMO, ISTN, IYR, MON, IDAY, IHR, NLEV, ALAT, ALON, ICLD, ICHT, ICLTYP, ICMTYP, ICHTYP, Q0, PPTBL, DRY, WET

where

IWMO = WMO station identifier
ISTN = station number
IYR = year of observation
MON = month of observation

IDAY = day of observation
IHR = hour of observation
NLEV = number of levels in atmosphere for which there are data
ALAT = latitude of observation
ALON = longitude of observation
ICLD = cloud cover
ICHT = cloud height
ICLTYP = low cloud type
ICMTYP = medium level cloud type
ICHTYP = high cloud type
Q0 = surface specific humidity
PPTBL = precipitable water content
DRY = surface air temperature
WET = surface wet bulb temperature

(c) COMMON/DATA/D(384) which is the read buffer for the profile. Note the array D is EQUIVALENCE (HDR(1),D(1)), where HDR is INTEGER*2 HDR(18).

Appendix B

The radiative transfer code / File descriptions

In this appendix the contents, form of data storage and size of binary files used by the programs to simulate the satellite measurements are described. All files have direct access. The files are listed below in alphabetic order of the file type and lowercase letters indicate a variable string, the contents of which uniquely identify a particular file.

File

name = yyyyyy.ATT
record length = 1024 real words (4096 bytes)
contents = spectra of atmospheric attenuation (generated by RADPM)
size = dependent on wavenumber interval and number of atmospheric profiles being processed – for channel 4 or 5, each profile requires 32 blocks of disk space

name = xxxRS.BIN
record length = 384 real words (1536 bytes)
contents = atmospheric profiles
size = dependent on number of atmospheric profiles (each profile requires one record) – for description of how file contents are to be interpreted see description of subroutine INPROF (A.6) (each record requires 3 blocks of disk space)

name = ATTCHb.BIN*
record length = 1024 real words (4096 bytes)
contents = precomputed atmospheric attenuation data in wavenumber interval of AVHRR channel 'b' (= 3, 4, 5)
size = dependent on wavenumber interval - see footnote

name = yyyyyy.CHR
record length = 1024 real words (4096 bytes)
contents = spectra of AVHRR channel radiance measurement (generated by BRIPM)
size = dependent on wavenumber interval and number of atmospheric profiles being processed - for channel 4 or 5, each profile requires 32 blocks of disk space

name = yyyyyy.DNR
record length = 1024 real words (4096 bytes)
contents = spectra of downwelling atmospheric radiance (generated by RADPM)
size = dependent on wavenumber interval and number of atmospheric profiles being processed - for channel 4 or 5, each profile requires 32 blocks of disk space

* The precomputed atmospheric attenuation data are stored as a sequence of six arrays at each of the five reference pressure values (1000, 800, 600, 400, 200 mbar) [see Sect. 3 of main report]. The number of 1024-word records needed for each array depends on the wavenumber interval of each channel, and is 30 for channel 3, 12 for channel 4 and 9 for channel 5. The sequence of arrays is

1 - linear term of the temperature dependence of the water vapour monomer absorption,
2 - water vapour monomer absorption at the reference pressure and temperature
3 - quadratic term of the temperature dependence of the water vapour monomer absorption,
4 - linear term of the temperature dependence of the absorption of carbon dioxide and well-mixed gasses
5 - absorption of carbon dioxide and well-mixed gasses at the reference pressure and temperature
6 - quadratic term of the temperature dependence of the absorption of carbon dioxide and well-mixed gasses.

The sequence is then repeated for each of the reference pressure levels.

name NaaCHb.RAD
record length = 1024 real words (4096 bytes)
contents = look-up table to convert radiances measured in channel 'b' of AVHRR on satellite NOAA-'aa' to temperatures (generated by TTORAD)
size = 1 record (i.e. 8 disk blocks)

name = yyyyyy.RAD
record length = 1024 real words (4096 bytes)
contents = spectra of total upwelling radiance at the satellite (generated by BRIPM)
size = dependent on wavenumber interval and number of atmospheric profiles being processed - for channel 4 or 5, each profile requires 32 blocks of disk space

name = NaaCHb.TRF
record length = 1024 real words (4096 bytes)
contents = channel spectral response function for channel 'b' of AVHRR on satellite NOAA-'aa'
size = dependent on wavenumber interval - 32 blocks required for 'b' = 4,5

name = xxxxxx.TRN
record length = 1024 real words (4096 bytes)
contents = spectra of atmospheric transmission (generated by ATRAN)
size = dependent on wavenumber interval and number of atmospheric profiles being processed - for channel 4 or 5, each profile requires 32 blocks of disk space

name = yyyyyy.UPR
record length = 1024 real words (4096 bytes)
contents = spectra of upwelling atmospheric radiance (generated by RADPM)
size = dependent on wavenumber interval and number of atmospheric profiles being processed - for channel 4 or 5, each profile requires 32 blocks of disk space

Appendix C

The radiative transfer code / Timing estimates

Of the programs that simulate the satellite measurements, only RADPM requires significant CPU time. All others run quickly enough to be used in an interactive mode. The time requirements of RADPM are linearly dependent on the number of atmospheric profiles being processed. For the split-window simulations (channels 4 and 5 of AVHRR), each profile requires 60 s of VAX8600 CPU time for channel 4 and 38 s for channel 5. Actual residence times of the program will be longer depending on the work load of the computer at the time.

Initial Distribution for SR-137

Ministries of Defence	
JSPHQ Belgium	2
DND Canada	10
CHOD Denmark	8
MOD France	8
MOD Germany	15
MOD Greece	11
MOD Italy	10
MOD Netherlands	12
CHOD Norway	10
MOD Portugal	2
MOD Spain	2
MOD Turkey	5
MOD UK	20
SECDEF US	68
NATO Authorities	
Defence Planning Committee	3
NAMILCOM	2
SACLANT	3
SACLANTREPEUR	1
CINCWESTLANT/ COMOCEANLANT	1
COMSTRIKFLTANT	1
CINCIBERLANT	1
CINCEASTLANT	1
COMSUBACLANT	1
COMMAIREASTLANT	1
SACEUR	2
CINCNORTH	1
CINCSOUTH	1
COMNAVSOUTH	1
COMSTRIKFORSOUTH	1
COMEDCENT	1
COMMARAIRMED	1
CINCHAN	3
SCNR for SACLANTCEN	
SCNR Belgium	1
SCNR Canada	1
SCNR Denmark	1
SCNR Germany	1
SCNR Greece	1
SCNR Italy	1
SCNR Netherlands	1
SCNR Norway	1
SCNR Portugal	1
SCNR Turkey	1
SCNR UK	1
SCNR US	2
French Delegate	1
SECGEN Rep. SCNR	1
NAMILCOM Rep. SCNR	1
National Liaison Officers	
NLO Canada	1
NLO Denmark	1
NLO Germany	1
NLO Italy	1
NLO UK	1
NLO US	1
NLR to SACLANT	
NLR Belgium	1
NLR Canada	1
NLR Denmark	1
NLR Germany	1
NLR Greece	1
NLR Italy	1
NLR Netherlands	1
NLR Norway	1
NLR Portugal	1
NLR Turkey	1
NLR UK	1
Total external distribution	250
SACLANTCEN Library	10
Stock	20
Total number of copies	280

END

DATE
FILMED

10-88